AD-A112 371 OHIO STATE UNIV COLUMBUS ELECTROSCIENCE LAB F/G 20/3
HIGH FREQUENCY SCATTERING BY CURVED SURFACES.(U)
JUN 74 P H PATHAK, R J MARHEFKA, W D BURNSIDE N62269-72-C-0354
UNCLASSIFIED ESL-3390-5 NL

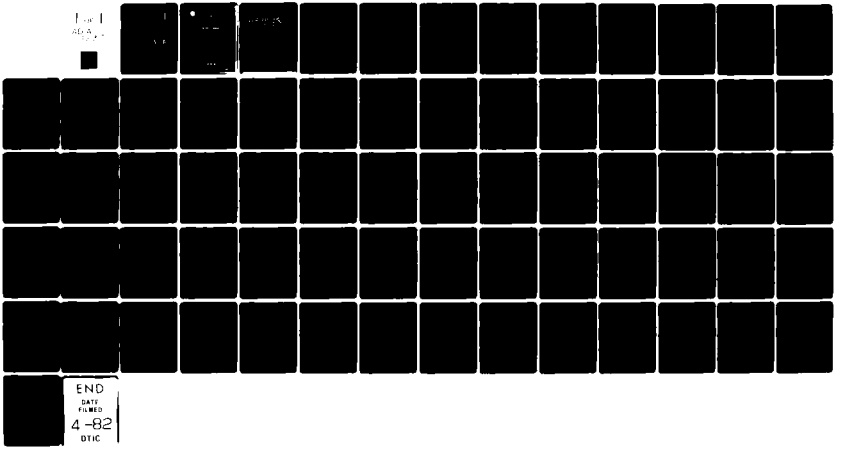

END
DATE FILMED
4-82
DTIC

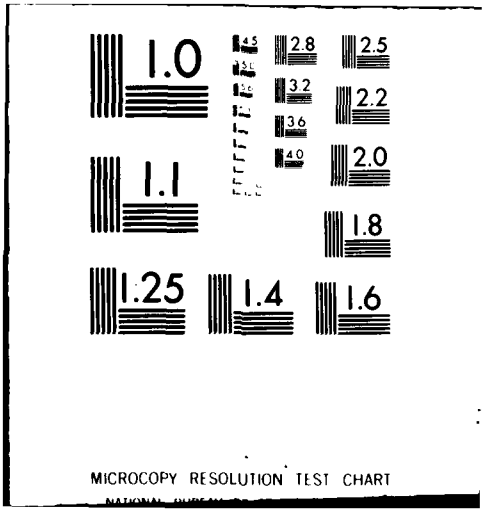
1.0
2.8
2.5
3.2
2.2
3.6
4.0
2.0
1.1
1.8
1.25
1.4
1.6
MICROCOPY RESOLUTION TEST CHART

PHOTOGRAPH THIS SHEET

A112 371

DTIC ACCESSION NUMBER

II

LEVEL

INVENTORY

Ohio State Univ., Columbus
ElectroScience Lab.

High Freguency Scattering by Curved Surfaces

Jun. 74

DOCUMENT IDENTIFICATION

Contract N62269-22-C-0354 Rept. No. ESL-3390-5

DISTRIBUTION STATEMENT A
Approved for public release;
Distribution Unlimited

DISTRIBUTION STATEMENT

ACCESSION FOR	
NTIS GRA&I	X
DTIC TAB	
UNANNOUNCED	
JUSTIFICATION	
Per Ltr. on File	
FL-88, Acq.# 82-0024(c) tnw (d)	
BY dtd 26 Jan. '82	
DISTRIBUTION /	
AVAILABILITY CODES	
DIST	AVAIL AND/OR SPECIAL
A	

DISTRIBUTION STAMP

DTIC
ELECTE
S MAR 24 1982 D
D

DATE ACCESSIONED

82 03 08 147

DATE RECEIVED IN DTIC

PHOTOGRAPH THIS SHEET AND RETURN TO DTIC-DDA-2

DTIC FORM OCT 79 70A

DOCUMENT PROCESSING SHEET

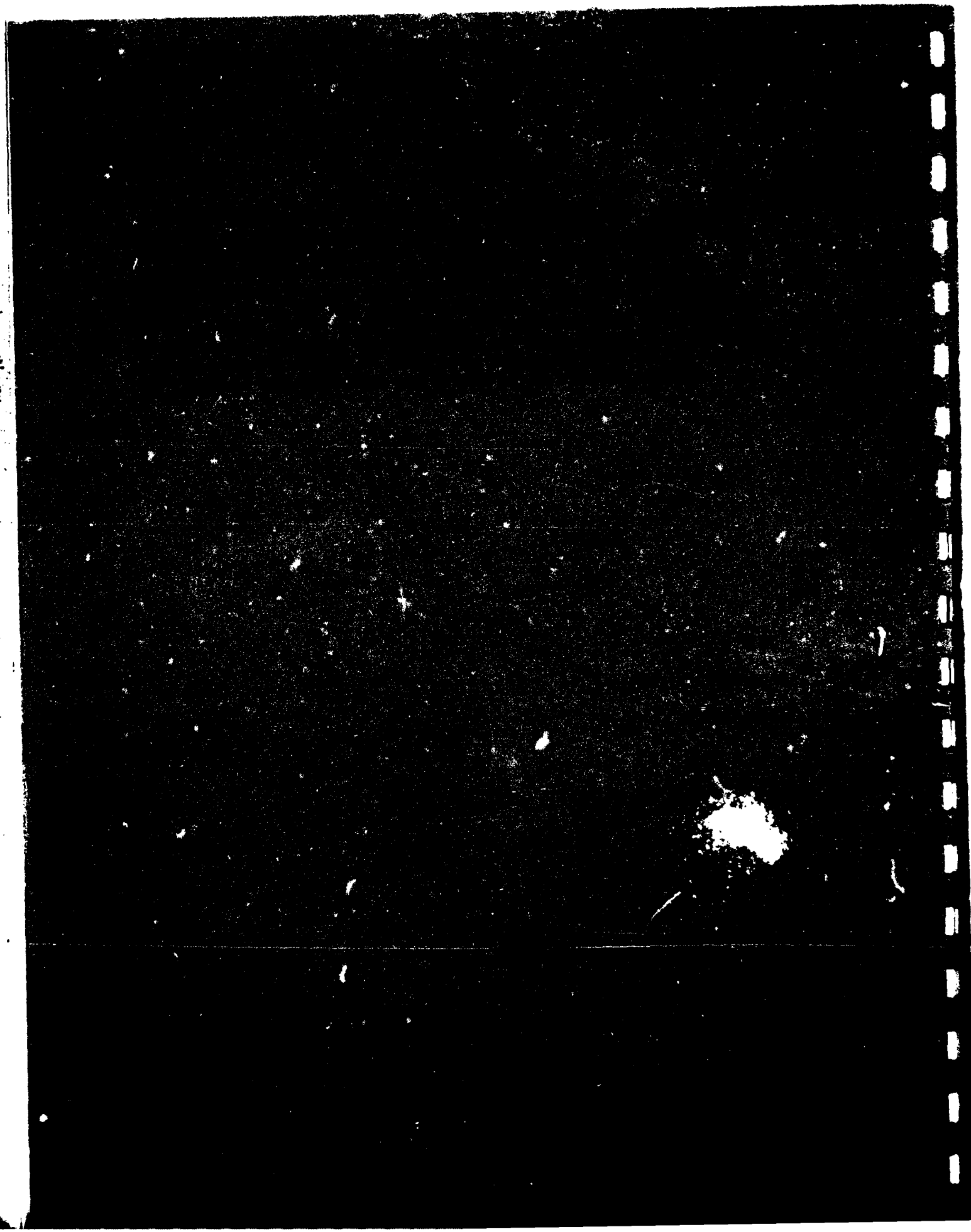

HIGH FREQUENCY SCATTERING BY CURVED SURFACES

P. H. Pathak
R. J. Marhefka
W. D. Burnside

TECHNICAL REPORT 3390-5

June 1974

Contract N62269-72-C-0354

Naval Air Development Center
Warminster, Pa. 18974

UNCLASSIFIED

SECURITY CLASSIFICATION OF THIS PAGE *(When Data Entered)*

REPORT DOCUMENTATION PAGE

READ INSTRUCTIONS BEFORE COMPLETING FORM

1. REPORT NUMBER	2. GOVT ACCESSION NO. / 3. RECIPIENT'S CATALOG NUMBER
4. TITLE *(and Subtitle)*: HIGH FREQUENCY SCATTERING BY CURVED SURFACES	5. TYPE OF REPORT & PERIOD COVERED: Technical Report
	6. PERFORMING ORG. REPORT NUMBER: ESL 3390-5
7. AUTHOR(s): P. H. Pathak, R. J. Marhefka, W. D. Burnside	8. CONTRACT OR GRANT NUMBER(s): Contract N62269-72-C-0354
9. PERFORMING ORGANIZATION NAME AND ADDRESS: The Ohio State University ElectroScience Lab, Department of Electrical Engineering, Columbus, Ohio 43212	10. PROGRAM ELEMENT, PROJECT, TASK AREA & WORK UNIT NUMBERS
11. CONTROLLING OFFICE NAME AND ADDRESS: Naval Air Development Center, Warminster, Pa. 18974	12. REPORT DATE: June 1974
	13. NUMBER OF PAGES: 61
14. MONITORING AGENCY NAME & ADDRESS *(if different from Controlling Office)*	15. SECURITY CLASS. *(of this report)*: Unclassified
	15a. DECLASSIFICATION/DOWNGRADING SCHEDULE

16. DISTRIBUTION STATEMENT *(of this Report)*

DISTRIBUTION STATEMENT A
Approved for public release; Distribution Unlimited

17. DISTRIBUTION STATEMENT *(of the abstract entered in Block 20, if different from Report)*

18. SUPPLEMENTARY NOTES

19. KEY WORDS *(Continue on reverse side if necessary and identify by block number)*

Curved surface diffraction
High frequency analysis
Transition region
Near zone scattering
Wing mounted antenna
Fuselage scattering

20. ABSTRACT *(Continue on reverse side if necessary and identify by block number)*

This report deals with the geometrical theory of diffraction (GTD) solution to the problem of plane wave high frequency (h.f.) scattering by a smooth, perfectly-conducting cylindrical surface. According to the GTD, the surface diffracted rays accurately describe the field behavior deep in the shadow region behind the obstacle; whereas, the incident and reflected rays adequately describe the field in the lit region sufficiently far from the optical shadow boundary. These ray solutions fail within the transition region adjacent to the shadow boundary; hence, an approximate h.f.

DD FORM 1 JAN 73 1473 EDITION OF 1 NOV 65 IS OBSOLETE

UNCLASSIFIED

SECURITY CLASSIFICATION OF THIS PAGE *(When Data Entered)*

20. solution is developed for describing the field within the transition region. The usefulness and the accuracy of this transition region solution is illustrated by analyzing the h.f. plane wave scattering by a 2-D cylindrically capped thick half plane, and a 2-D circular cylinder (for which an exact solution is available for comparison), respectively. The present transition region solution is in a form which facilitates its generalization to treat 2-D, and 3-D convex surfaces of non-constant curvature. A simple example of this generalization is illustrated by analyzing the h.f. plane wave scattering by a 3-D, hemispherically capped semi-infinite circular cylinder. The work described in this report is important to the analysis of the problem of h.f. scattering by a finite elliptic cylinder excited by a finite source; this problem is directly relevant to a study of the effect of an aircraft fuselage on the performance of wing mounted antennas.

ABSTRACT

This report deals with the geometrical theory of diffraction (GTD) solution to the problem of plane wave high frequency (h.f.) scattering by a smooth, perfectly-conducting cylindrical surface. According to the GTD, the surface diffracted rays accurately describe the field behavior deep in the shadow region behind the obstacle; whereas, the incident and reflected rays adequately describe the field in the lit region sufficiently far from the optical shadow boundary. These ray solutions fail within the transition region adjacent to the shadow boundary; hence, an approximate h.f. solution is developed for describing the field within the transition region. The usefulness and the accuracy of this transition region solution is illustrated by analyzing the h.f. plane wave scattering by a 2-D cylindrically capped thick half plane, and a 2-D circular cylinder (for which an exact solution is available for comparison), respectively. The present transition region solution is in a form which facilitates its generalization to treat 2-D, and 3-D convex surfaces of non-constant curvature. A simple example of this generalization is illustrated by analyzing the h.f. plane wave scattering by a 3-D, hemispherically capped semi-infinite circular cylinder. The work described in this report is important to the analysis of the problem of h.f. scattering by a finite elliptic cylinder excited by a finite source; this problem is directly relevant to a study of the effect of an aircraft fuselage on the performance of wing mounted antennas.

TABLE OF CONTENTS

I. INTRODUCTION

On-aircraft antenna pattern performance is very much dependent on the scattered field from the fuselage. This point was emphasized in the analysis of fuselage mounted antennas[1]. For certain sectors of the volumetric pattern, the fuselage may even play a more dominant role for antennas mounted off the fuselage. This is especially true in the azimuth plane for wing mounted antennas. For many years scale model measurements have been used to study these effects; however, such measurements are both time consuming and expensive. On the other hand, numerical solutions have been successfully applied for the past few years to study designs and locations for fuselage-mounted antennas. Fundamentally, the analyses developed for fuselage-mounted antennas can be extended to handle off-fuselage antennas.

Based on the numerical techniques previously developed[1,2,3], it is proposed that similar solutions be investigated for wing-mounted antennas. Specifically, the near-zone scattered field solutions for a finite flat plate and finite circular cylinder have already been developed[1]. However, these models are not as versatile as desired. Further the finite cylinder is limited to electrically small radii due to use of a modal solution. Consequently, it is proposed that a high frequency solution for sources in the near zone of a finite elliptic cylinder be employed. This model allows for variations in the cross-section of the theoretical model and is not limited to lower frequencies, i.e., to electrically small bodies.

The theoretical solutions necessary to analyze this problem are developed in this report in terms of the solution to the scattering by a two-dimensional circular cylinder. The geometric optics solution satisfactorily handles the lit zone; whereas, the geometrical theory of diffraction can be used in the deep shadow. However, both solutions fail on and near the shadow boundary; hence, an approximate asymptotic high

frequency result is developed for analyzing the field within the transition region adjacent to the shadow boundary. Further, the solutions developed herein can be extended to handle arbitrary curved surfaces including the three-dimensional case. These solutions will provide the necessary theoretical background to complete the study of a finite elliptic cylinder which will be treated in a future report.

The canonical problem that is treated involves the calculation of the total high frequency field which is observed at a finite distance from a convex, cylindrically shaped diffracting obstacle when it is illuminated by an incident plane wave. This problem is directly equivalent to the relevant problem of calculating the radiation pattern of a source located at a finite distance from the same smooth, convex diffracting obstacle via the reciprocity theorem for electromagnetic fields.

II. HIGH FREQUENCY SCATTERING BY SOME SPECIAL 2-D, SMOOTH, CYLINDRICAL SURFACES

This section deals with the high frequency scattering of electromagnetic waves by a smooth, two-dimensional perfectly-conducting cylindrical surface. In this study, special emphasis is given to the region near the shadow boundary. A solution is desired which can be generalized (based on high frequency approximations) to treat the scattering by three-dimensional surfaces without having to solve additional canonical problems. The general problem of the diffraction of waves by smooth, convex surfaces for grazing angles, (i.e., in the transition region adjacent to a shadow boundary) is difficult to solve and it has been the subject of investigation by various authors[4] who considered some general cases; however, owing to the mathematical complexity of their solutions, their results do not appear to be in a form tractable for application to engineering problems of practical interest. For the special case of high frequency plane wave diffraction by a perfectly-conducting circular cylinder, Goriainov[5] has obtained results

for grazing angles which are in a form suitable for numerical calculations. Wait and Conda[6] extended Goriainov's high frequency results to treat the plane wave diffraction by a circular cylinder with an impedance type boundary condition; they also included the case of spherical wave incidence. Most of the previous works on curved surface diffraction for grazing angles including the work in References [5] and [6] make use of Fock integrals introduced by Fock in his fundamental work on diffraction by smooth surfaces (many of Fock's papers are listed in Reference [4]). Wait and Conda[6] indicate that their high frequency (h.f.) solution for the plane wave diffraction (for grazing angles) by a circular cylinder can be interpreted as being the superposition of the result based on Kirchhoff diffraction theory, and a second term which is viewed as a correction to the Kirchhoff theory. This observation by Wait and Conda[6] constitutes the physical basis for the development pursued in this report to arrive at a result which could be simply extended to treat the h.f. scattering (in the transition zone) by arbitrary 2-D and 3-D smooth, convex, conducting surfaces. The decomposition of the field scattered by the 2-D cylinder into a sum of a Kirchhoff diffraction term and a surface diffracted term (viewed as a correction to Kirchhoff theory) as observed by Wait and Conda[6] was also indicated by Fock (see pp. 194-196 of Reference [6]). In his work on the 3-D scattering problem of the Fresnel diffraction by a sphere for the special case of source and observer raised to small heights above the sphere, Fock expressed the scattered field in terms of a superposition of two integrals; one of these integrals happened to be independent of the electrical properties of the surface, and the other explicitly contained the surface properties and its associated electrical properties. Fock then showed that the integral for the scattered field which is independent of the electrical properties reduced to a Fresnel edge diffraction term; this term corresponds to Kirchhoff diffraction. On the other hand, the integral which depended on the electrical properties of the surface was shown by Fock to yield the surface diffracted term (which is viewed as a correction to Kirchhoff diffraction). Consequently, it is believed that the basis of our analytical development given in this report is justified in view of the above remarks.

Since the circular cylinder has two penumbral regions on its surface as shown in Fig. 1, one needs to isolate the contribution to the field

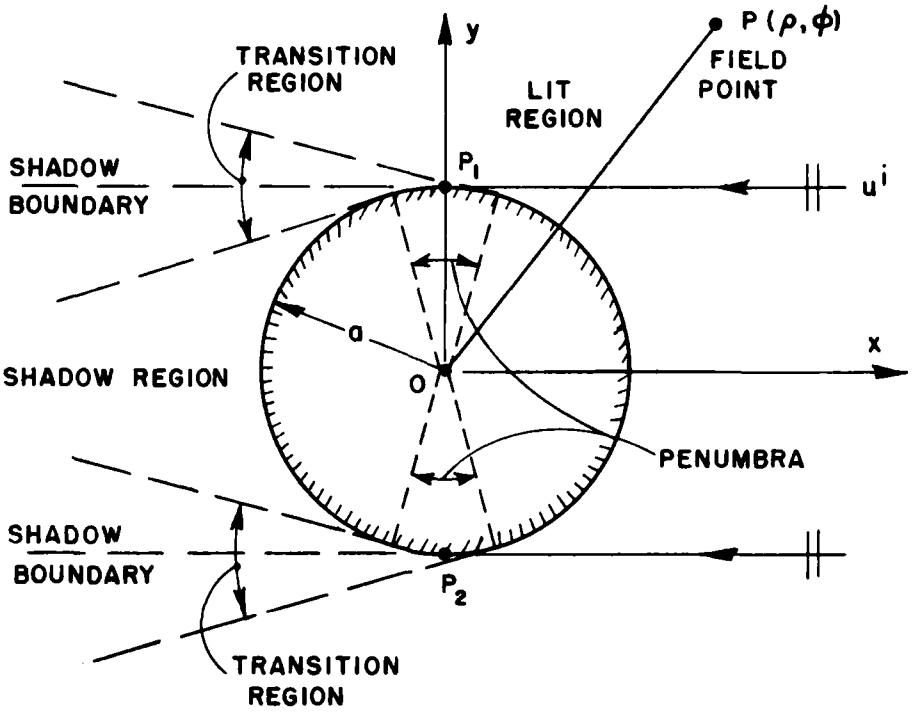

Fig. 1. Geometry for the plane wave scattering by a circular cylinder.

from each of these penumbral regions in order to allow an extension of the circular cylinder analysis to treat the h.f. waves diffracted from a single penumbral region, such as that which occurs on a smooth convex surface of the nose of an aircraft when it is illuminated by a wing mounted antenna. One notes that the angular extent of the penumbral regions and the transition regions (which lie adjacent to the shadow boundaries) is approximately $2(ka/2)^{-1/3}$ in radians (ka = circumference of the cylinder in wavelengths). In Section II-A below, it is shown that the h.f. field contributions arising from each of the two penumbral regions on a circular cylinder can be identified, and separated in a manner which enables one to calculate the h.f. field within a transition region which is

associated with a single penumbral region on the cylinder. Such a decomposition of the circular cylinder solution facilitates the analysis of the problem of h.f. plane wave diffraction by the convex portion of the 2-D, perfectly-conducting, rounded-end, thick-screen configuration of Fig. 2.

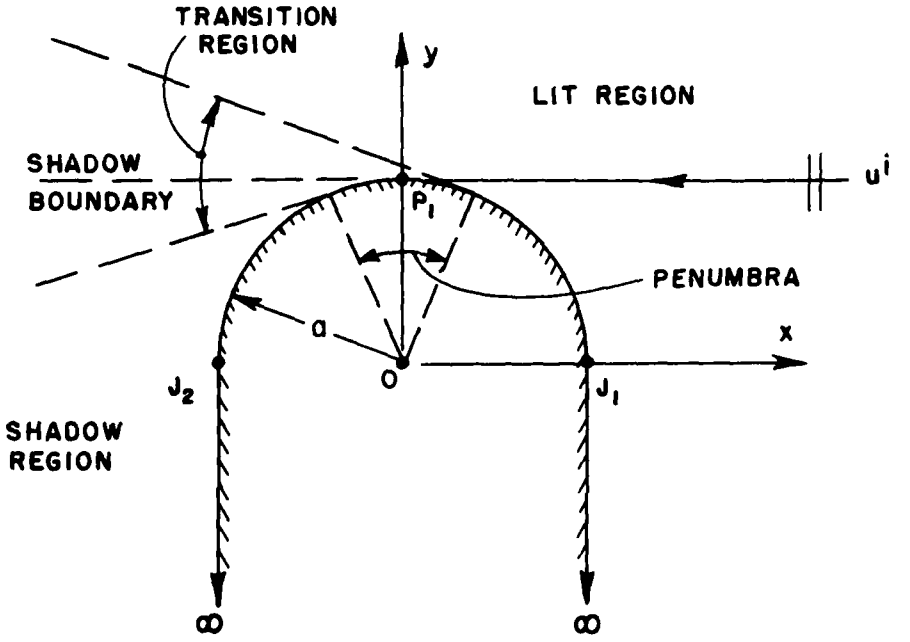

Fig. 2. Geometry associated with the plane wave scattering by a cylindrically tipped thick half-plane.

One notes that the configuration of Fig. 2 consists of a half cylinder of radius (a) which is smoothly joined to a thick half plane whose thickness is 2a. The curve defining the boundary of the configuration in Fig. 2 is not closed, and therefore there exists only one penumbral region on the convex portion of this scattering geometry as illustrated in Fig. 2. The results for the h.f. scattering by the canonical configuration of Fig. 2 are given in Section II-B; it is conjectured that these results can be extended in a systematic fashion to treat the h.f. scattering by arbitrary convex conducting surfaces if one employs the hypothesis valid at high

frequencies, namely that h.f. diffraction and reflection are local phenomena (i.e., h.f. diffraction and reflection mechanisms are localized to the immediate vicinity of certain points on the surface of the scatterer, which correspond to points of diffraction and reflection, respectively). An extension of the results in Section II-B for the 2-D canonical configuration of Fig. 2 to analyze the problem of h.f. scattering by a 3-D, perfectly-conducting hemispherically capped, semi-infinite circular cylinder geometry is indicated in Section III. The more general extension of the results of Section II-B to handle arbitrary curved surfaces will be the topic of a future investigation.

A. Transition Region Solution for the H.F. Plane Wave Scattering by a Circular Cylinder

Let the total field, u in a region external to the 2-D perfectly-conducting circular cylinder of Fig. 1 be the superposition of the incident field (u^i) and the scattered field (u^s). In the case of TM_z excitation, the electric field associated with the incident plane wave (u^i) is entirely parallel to the axis of the cylinder (i.e., along z); furthermore, the total electric field denoted by u is also entirely z-directed. Similarly, for the TE_z excitation of the cylinder, u^i and u represent the incident and total magnetic field intensities, respectively, which are entirely z-directed. Let u_s denote the value of u for the TM_z case, and let u_h denote the value of u for the TE_z case. Then, $u_s = u_s^{i+s}$ satisfies the 2-D homogeneous, reduced wave equation in the region exterior to the cylinder, i.e.,

$$(1) \qquad (\nabla_t^2 + k^2)\, u_s = 0,$$

subject to the boundary conditions;

$$(2a) \qquad u_s = 0 \quad \text{on the cylinder,}$$

or

(2b) $$\frac{\partial u_h}{\partial \rho} = 0 \quad \text{on the cylinder.}$$

In addition,

(3) u_s^s must satisfy the Sommerfeld radiation condition as $\rho \to \infty$ for an $e^{i\omega t}$ time convention which is assumed and suppressed.

The incident plane wave field is given by:

(4) $$u_s^i = e^{ikx}.$$

The quantity k present in the above equations refers to the free space wave number. Since Eq. (4) satisfies the reduced wave equation, it follows from Eq. (1) that u_s^s must also satisfy the reduced wave equation. An application of the 2-D Green's theorem to the region surrounding the cylinder of Fig. 1 yields

(5) $$u(P) = u^i(P) + \int_0^{2\pi} \left[u(P') \frac{\partial G_0(P|P')}{\partial \rho'} - G_0(P|P') \frac{\partial u(P')}{\partial \rho'} \right]_{\rho'=a} a\,d\phi'$$

where $G_0(P|P')$ is the 2-D free-space Green's function:

(6) $$G_0(P|P') = -\frac{i}{4} H_0^{(2)}(k|\bar{\rho} - \bar{\rho}'|).$$

The parameter $(\bar{\rho})$ denotes the field point position vector of $P = P(\rho,\phi)$; and $\bar{\rho}'$ denotes the cylindrical surface position vector of $P' = P'(\rho',\phi')$ with $\rho' = a$ on the cylinder. Clearly, the integral term on the RHS of Eq. (5) is the scattered field u^s. Then, from Eqs. (2), (3) and (5)

(7a) $$u_s^s(P) = -\int_0^{2\pi} \left[G_0(P|P') \frac{\partial u_s(P')}{\partial \rho'} \right]_{\rho'=a} a\,d\phi',$$

and

(7b) $$u_h^s(P) = \int_0^{2\pi} \left[u_h(P') \frac{\partial G_0(P|P')}{\partial \rho'} \right]_{\rho'=a} a\,d\phi',$$

with the understanding that

(8a) $$u_s = u_s^i + u_s^s, \quad \text{for the } TM_z \text{ case,}$$

and

(8b) $$u_h = u_h^i + u_h^s, \quad \text{for the } TE_z \text{ case.}$$

It is well known[4,5] that a valid asymptotic h.f. approximation for the surface field which is induced within the penumbral regions on the surface of a circular cylinder, when it is illuminated by a plane wave, is given by the following set of equations:

(9a) $$\left[\frac{\partial u_s}{\partial \rho'}\right]_{\rho'=a} \approx - \sum_{\ell=0}^{\infty} k \left(\frac{2}{ka}\right)^{1/3} \left[\tilde{g}(\hat{\xi}_1)\, e^{-ika\hat{\psi}_1} + \tilde{g}(\hat{\xi}_2)\, e^{-ika\hat{\psi}_2}\right],$$

and

(9b) $$\left[u_h\right]_{\rho'=a} \approx \sum_{\ell=0}^{\infty} \left[g(\hat{\xi}_1)\, e^{-ika\hat{\psi}_1} + g(\hat{\xi}_2)\, e^{-ika\hat{\psi}_2}\right].$$

The functions which appear above are the universal Fock functions defined by

(10a),(10b) $$\tilde{g}(\hat{\xi}) = \frac{1}{\sqrt{\pi}} \int_{\Gamma_1} \frac{e^{-i\hat{\xi}\tau}}{w_2(\tau)}\, d\tau \quad ; \quad g(\hat{\xi}) = \frac{1}{\sqrt{\pi}} \int_{\Gamma_1} \frac{e^{-i\hat{\xi}\tau}}{w_2'(\tau)}\, d\tau \quad ,$$

in which the Fock-type Airy function $w_2(\tau)$, and its derivative $w_2'(\tau)$ are defined by:

(11a),(11b) $$w_2(\tau) = \frac{1}{\sqrt{\pi}} \int_{\Gamma_2} e^{\tau z - \frac{z^3}{3}}\, dz \quad ; \quad w_2'(\tau) = \frac{1}{\sqrt{\pi}} \int_{\Gamma_2} z\, e^{\tau z - \frac{z^3}{3}}\, dz.$$

The Fock parameters $\hat{\xi}_1$ and $\hat{\xi}_2$ are given by:

(12a),(12b) $$\hat{\xi}_1 = \left(\frac{ka}{2}\right)^{1/3} \hat{\psi}_1 \quad ; \quad \hat{\xi}_2 = \left(\frac{ka}{2}\right)^{1/3} \hat{\psi}_2 \quad ,$$

with $\hat{\psi}_1 = |\phi'| - \pi/2 + 2\pi\ell$, and $\hat{\psi}_2 = 3\pi/2 - |\phi'| + 2\pi\ell$. The contours of integration Γ_1 and Γ_2 for the integrals in Eqs. (10a,10b) and (11a,11b) are shown in Fig. 3.

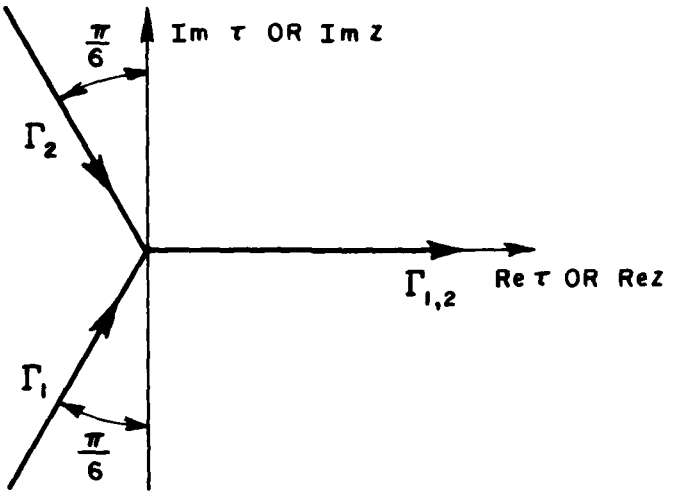

Fig. 3. Contours of integration for the Fock and Airy functions.

The two terms on the RHS of Eq. (9a) and Eq. (9b) are commonly viewed as two oppositely traveling creeping waves (associated with the surface current) on the cylinder which have encircled the cylinder ℓ times. If $(ka)^{1/3}\pi >> 1$, the effect of the multiply encircling terms is negligible and the inclusion of only the ℓ=0 term is sufficient. In this report, one is concerned with eventually applying the appropriate circular cylinder results to the semi-infinite geometrical configuration of Fig. 2; hence, it is meaningful to retain only the ℓ=0 term in the present analysis.

Employing the far-zone approximation to $G_0(P|P')$ leads to the following results for $G_0(P|P')$ and $\frac{\partial G_0(P|P')}{\partial \rho'}$:

$$(13) \qquad [G_0(P|P')]_{\rho'=a} \sim -\frac{i}{4}\sqrt{\frac{2}{\pi k\rho}}\, e^{-i(k\rho-\pi/4)}\, e^{ika\cos(\phi-\phi')} \quad ,$$

$$(14) \qquad \left[\frac{\partial G_o(P|P')}{\partial \rho'}\right]_{\rho'=a} \sim \frac{k}{4}\sqrt{\frac{2}{\pi k\rho}}\ \cos(\phi-\phi')\ e^{-i(k\rho-\pi/4)}\ e^{ika\cos(\phi-\phi')} \quad .$$

The far-zone approximation implies that $k|\bar{\rho} - \bar{\rho}'| >> 1$ and $\rho >> (\rho'=a)$ in Eqs. (7a,7b).

It is now possible to obtain asymptotic approximations to the integrals in Eq. (7a) and Eq. (7b) for the scattered fields subject to the restrictions indicated in Eqs. (13) and (14). Employing Eqs. (9a) and (13) in Eq. (7a), and expanding the exponential part of the integrand about a stationary point allows one to write the integral in terms of functions which are tabulated; thus, one is led to the following result for $|\phi - \pi| << (\frac{ka}{2})^{-1/3}$:

$$(15) \qquad u_s^s(P) \sim -\frac{e^{-ik\rho}}{\sqrt{\rho}}\left[\left\{\sqrt{\frac{2}{\pi k}}\ e^{i\pi/4}\ \frac{\sin ka(\phi-\pi)}{(\phi-\pi)}\right\} + \right.$$

$$\left. + e^{-i\pi/4}\sqrt{\frac{2}{k}}\ (\frac{ka}{2})^{1/3}\left\{p^*(\xi_1)\ e^{-ika\psi_1} + p^*(\xi_2)\ e^{-ika\psi_2}\right\}\right].$$

A similar asymptotic solution for the integral in Eq. (7b) is obtained by incorporating Eq. (9b) and Eq. (14) in it's integrand; thus,

$$(16) \qquad u_h^s(P) \sim -\frac{e^{-ik\rho}}{\sqrt{\rho}}\left[\left\{\sqrt{\frac{2}{\pi k}}\ e^{i\pi/4}\ \frac{\sin ka(\phi-\pi)}{(\phi-\pi)}\right\} + \right.$$

$$\left. + e^{-i\pi/4}\sqrt{\frac{2}{k}}\ (\frac{ka}{2})^{1/3}\left\{q^*(\xi_1)\ e^{-ika\psi_1} + q^*(\xi_2)\ e^{-ika\psi_2}\right\}\right].$$

The results indicated in Eqs. (15) and (16) were obtained earlier by Goriainov[5], and Wait and Conda[6]. The universal functions $p^*(\xi)$ and $q^*(\xi)$ are the complex conjugates of the $p(\xi)$ and $q(\xi)$ functions defined by Logan[4,5,7] ($p^*(\xi) = G(\xi,q\to\infty)\ e^{i\pi/4}$ and $q^*(\xi) = G(\xi,q=0)\ e^{i\pi/4}$, where $G(\xi,q)$ has been introduced by Wait[6]). The functions $e^{-i\pi/4}\ p^*(\xi)$,

and $e^{-i\pi/4}\ q^*(\xi)$ are plotted in Figs. 4a and 4b, respectively. The arguments ξ_1 of the $p^*(\xi_1)$ and $q^*(\xi_1)$ functions are given by:
2 2 2

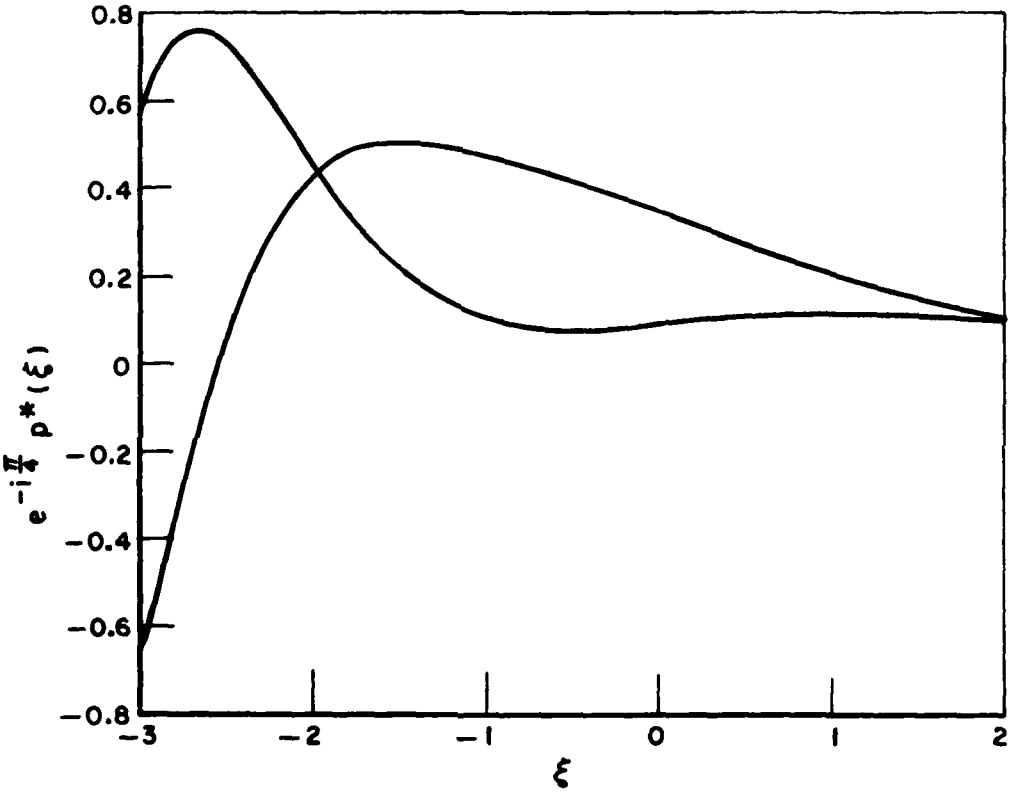

Fig. 4a. Plot of $e^{-i\pi/4}p^*(\xi)$ vs ξ based on Logan's tabulated data[7] for $p(\xi)$.

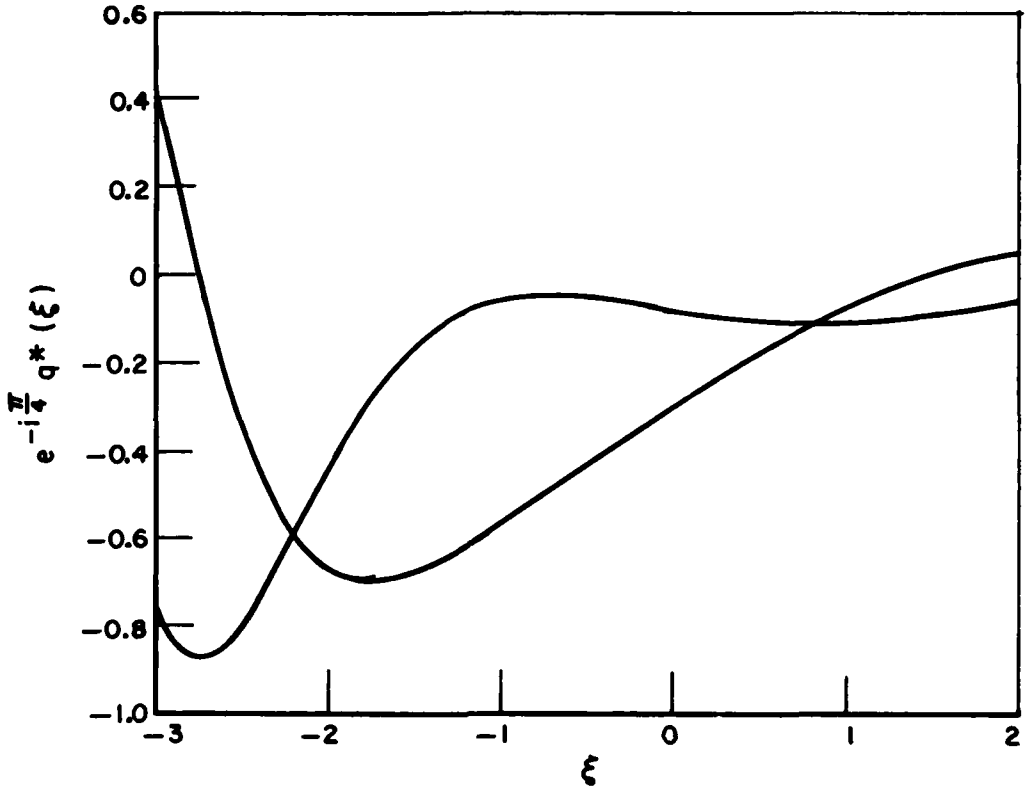

Fig. 4b. Plot of $e^{-i\pi/4}q^*(\xi)$ vs ξ based on Logan's tabulated data[7] for $q(\xi)$.

(17a,17b) $\xi_1 = (\frac{ka}{2})^{1/3}\psi_1$; $\xi_2 = (\frac{ka}{2})^{1/3}\psi_2$

with $\psi_1 = \phi - \pi$, and $\psi_2 = \pi - \phi$.

The details of the asymptotic approximation to the integrals in Eqs. (7a) and (7b) do not appear to be readily accessible in the literature, and are therefore given in Appendix I for the sake of completeness.

It has been pointed out by Wait and Conda[6] that the first term on the RHS of Eqs. (15) and (16) corresponds to Kirchhoff diffraction; whereas, the remaining terms may be viewed as a correction to the Kirchhoff

theory. The Kirchhoff result is independent of the electrical properties of the surface; it is obtained by assuming that the field scattered by the cylinder of Fig. 1 is equal to that scattered by a strip of the same geometrical cross-section (i.e., strip width = diameter of the cylinder) which is located at x=0 as in Fig. 5a. It is possible to provide a ray interpretation for the scattered fields given in Eqs. (15) and (16); the Kirchhoff term is composed of the field associated with the Kirchhoff diffracted rays which emanate from the edges P_1 and P_2 (of the strip) as illustrated in Fig. 5a; whereas, the terms involving $p^*(\xi_1)$ and $q^*(\xi_1)$ are the fields associated with the ray which is launched by the incident field at P_1 and shed along the forward tangent at P_3, after creeping a distance P_1P_3 on the cylinder ($P_1P_3 = a|\psi_1|$) as illustrated in Fig. 5b. A pseudo-ray interpretation[8] is possible for the terms $p^*(\xi_2)$ and $q^*(\xi_2)$ as illustrated in Fig. 5b, wherein the ray associated with these terms is launched at P_2, and is shed along the backward tangent at P_4 after creeping a distance P_2P_4 on the cylinder ($P_2P_4 = a|\psi_2| = a|\psi_1|$); this ray system unlike the ones described above, does not satisfy the generalized Fermat's principle which is employed in Keller's geometrical theory of diffraction[9], but it is nevertheless useful in visualizing the geometrical coordinates which are associated with the terms $p^*(\xi_2)\, e^{-ika\psi_2}$ and $q^*(\xi_2)\, e^{-ika\psi_2}$. In Fig. 5a, $u_1^k(P)$ denotes the Kirchhoff edge diffracted field emanating from P_1; similarly, $u_2^k(P)$ denotes the field arising from the edge P_2 so that

$$(18) \qquad u_1^k(P) + u_2^k(P) \approx -\frac{\sin ka(\phi-\pi)}{(\phi-\pi)} \sqrt{\frac{2}{\pi k}}\, e^{i\pi/4}\, \frac{e^{-ik\rho}}{\sqrt{\rho}}, \quad \text{for } \phi \approx \pi$$

corresponds to the Kirchhoff result which is contained in Eq. (15) and Eq. (16), respectively,

One is now able to identify the scattered fields which arise from the two isolated penumbral regions shown in Fig. 1. Specifically, the scattered field at P (in the close vicinity of $\phi=\pi$) arising from the penumbral region associated with P_1 is:

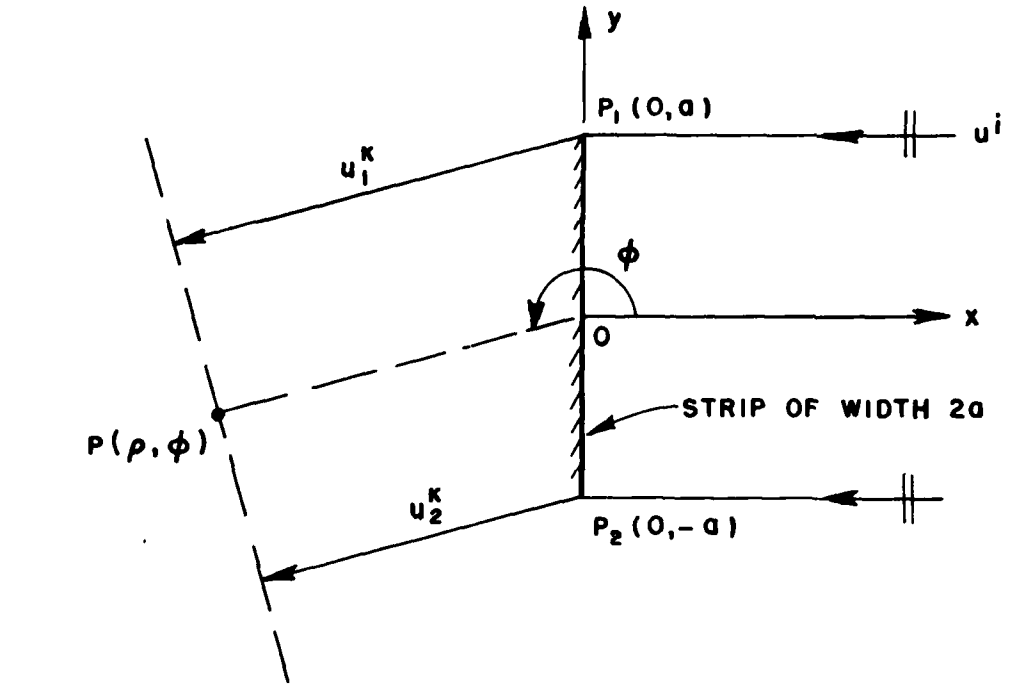

(a)

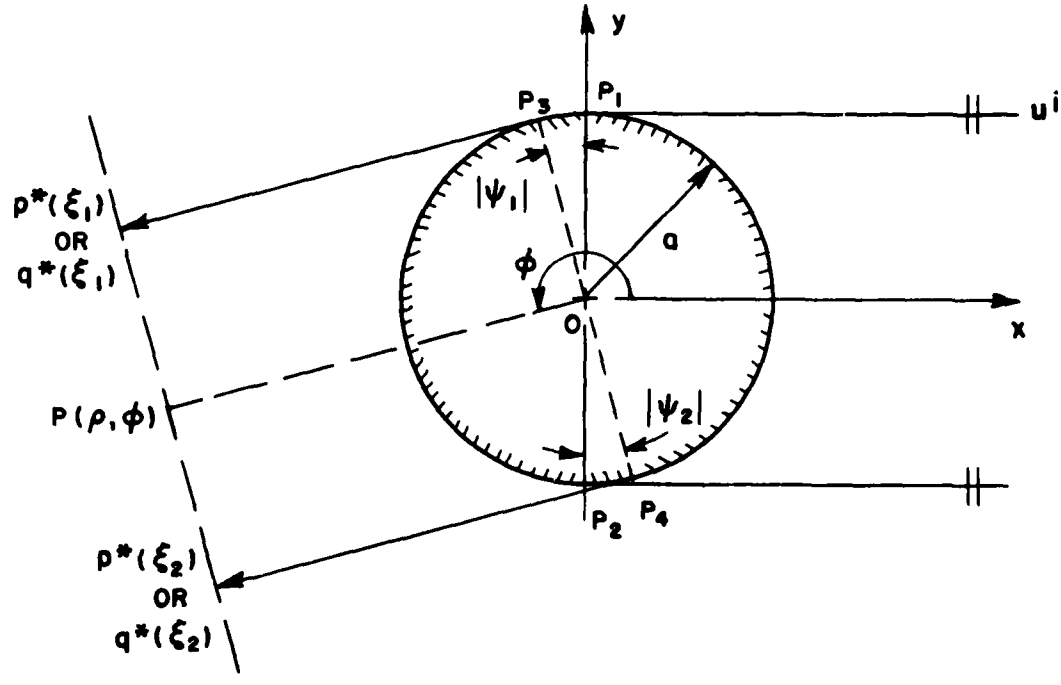

(b)

Fig. 5. Physical interpretation for the results in Eqs. (15) and (16).

(19a) $$u_s^s(P,P_1) \sim u_1^k(P) - e^{-i\pi/4}\sqrt{\frac{2}{k}}\left(\frac{ka}{2}\right)^{1/3} p^*(\xi_1)\, e^{-ika\psi_1}\frac{e^{-ik\rho}}{\sqrt{\rho}},$$

for the TM_z case and $\phi \gtrsim \pi$

(19b) $$u_h^s(P,P_1) \sim u_1^k(P) - e^{-i\pi/4}\sqrt{\frac{2}{k}}\left(\frac{ka}{2}\right)^{1/3} q^*(\xi_1)\, e^{-ika\psi_1}\frac{e^{-ik\rho}}{\sqrt{\rho}},$$

for the TE_z case and $\phi \gtrsim \pi$.

Similarly, the scattered field at P emanating from the penumbral region associated with P_2 is:

(20a) $$u_s^s(P,P_2) \sim u_2^k(P) - e^{-i\pi/4}\sqrt{\frac{2}{k}}\left(\frac{ka}{2}\right)^{1/3} p^*(\xi_2)\, e^{-ika\psi_2}\frac{e^{-ik\rho}}{\sqrt{\rho}},$$

for the TM_z case and $\phi \gtrsim \pi$

(20b) $$u_h^s(P,P_2) \sim u_2^k(P) - e^{-i\pi/4}\sqrt{\frac{2}{k}}\left(\frac{ka}{2}\right)^{1/3} q^*(\xi_2)\, e^{-ika\psi_2}\frac{e^{-ik\rho}}{\sqrt{\rho}},$$

for the TE_z case and $\phi \gtrsim \pi$.

Re-writing the RHS of Eq. (18) for $\phi \to \pi$, one obtains the following:

(21) $$-\frac{\sin ka(\phi-\pi)}{(\phi-\pi)}\sqrt{\frac{2}{\pi k}}\, e^{i\pi/4}\frac{e^{-ik\rho}}{\sqrt{\rho}} = \left[\frac{e^{-ika(\phi-\pi)}}{(\phi-\pi)} - \frac{e^{ika(\phi-\pi)}}{(\phi-\pi)}\right]\sqrt{\frac{1}{2\pi k}}\, e^{-i\pi/4}\frac{e^{-ik\rho}}{\sqrt{\rho}} .$$

One is now able to associate the first term on the RHS of Eq. (21) with u_1^k; likewise, the second term on the RHS of Eq. (21) corresponds to u_2^k. However, the individual terms $\pm\frac{e^{\mp ika(\phi-\pi)}}{(\phi-\pi)}$ on the RHS of Eq. (21) are unbounded at $\phi=\pi$ (even though the LHS of Eq. (21) remains finite); consequently, they must be replaced by the bounded Kirchhoff result for

u_1^k which is deduced from the result for the Kirchhoff diffraction by a conducting half-plane. The u_1^k term is now viewed as being the h.f. field diffracted from the edge P_1 of a half-plane located at x=0 for $-\infty<y\leq a$. Similarly, the u_2^k term is viewed as being the diffracted field from the edge P_2 of a half plane located at x=0 for $-a\leq y<\infty$. In doing so, one assumes that the h.f. fields diffracted by the strip in Fig. 5a is the superposition of the fields associated with rays diffracted from the edges P_1 and P_2 of two overlapping half planes (with their common domain of overlap = width of the strip); this assumption is reasonable since ka is assumed large. The Kirchhoff result for the field diffracted by the edge P_1 of a half-plane when a plane wave is normally incident on it is given in terms of a Kirchhoff edge diffraction coefficient, D_k as

$$u_1^k(P) \sim u^i(P_1)\, D_k(\phi)\, \frac{e^{-ik(\rho-a\sin\phi)}}{\sqrt{\rho}} \quad , \tag{22}$$

where $u^i(P_1)$ is unity, and

$$D_k(\phi) \equiv -\frac{i}{4}\sqrt{\frac{2}{\pi k}}\; e^{i\pi/4}\; (-\frac{2}{\sin\phi})\; F(X) \tag{23}$$

with

$$F(X) \equiv 2i|\sqrt{X}|e^{i|X|} \int_{|\sqrt{X}|}^{\infty} e^{-i\tau^2}\, d\tau \quad , \tag{24a}$$

and

$$X = 2k\rho\cos^2\frac{\phi}{2} \; . \tag{24b}$$

$u_1^k(P)$ of Eq. (22) with $D_k(\phi)$ as in Eq. (23) approaches the following result as $\phi\to\pi$:

$$u_1^k(P) \sim \left(\frac{e^{-ika(\phi-\pi)}}{(\phi-\pi)} \sqrt{\frac{1}{2\pi k}}\; e^{-i\pi/4}\; \frac{e^{-ik\rho}}{\sqrt{\rho}} \right) F(X) \quad , \tag{25}$$

which is identical to the first term on the RHS of Eq. (21) except for the additional factor F(X).

$$F(X) \approx (\sqrt{\pi X} - 2Xe^{i\pi/4}) \cdot e^{i(\pi/4 + X)}$$

as $\phi \to \pi$, thereby ensuring a bounded result for $u_1^k(P)$ of Eq. (22) at the shadow boundary corresponding to $\phi=\pi$. The derivation of the result in Eq. (22) is summarized in Appendix II. The function F(X) was introduced by Hutchins and Kouyoumjian[10] to describe the h.f. diffracted fields in the transition regions of the shadow and reflection boundaries associated with a perfectly conducting wedge illuminated by a plane wave. A plot indicating the behavior of F(X) is given in Fig. 6. The field $u_2^k(P)$ is similarly expressed in terms of D_k as

$$(26) \qquad u_2^k(P) \sim u^i(P_2)\, D_k(2\pi-\phi)\, \frac{e^{-ik(\rho+a\sin\phi)}}{\sqrt{\rho}}$$

which is also finite at $\phi=\pi$. The exponential phase factors $e^{\pm ika\sin\phi}$ in Eqs. (22) and (26) arise from choosing the origin as the phase reference. The results in Eqs. (22) and (26) facilitate the calculation of the Kirchhoff diffracted fields u_1^k and u_2^k over a greater angular region about the shadow boundary than just within the immediate neighborhood of the shadow boundary at $\phi=\pi$. It can be shown by a careful limiting operation that a superposition of Eqs. (22) and (26) also leads to the result on the LHS of Eq. (21) for $\phi \approx \pi$. In this limiting operation, the fields in Eq. (22) and Eq. (26) are initially assumed to emanate from P_1 and P_2, respectively to the far-zone field point P (in the vicinity of $\phi=\pi$) along nearly parallel ray paths which converge at P. Next, the field corresponding to this nearly parallel convergent ray system is allowed to approach the parallel ray system (of Fig. 5a) in the mathematical limit. One may thus employ the field representations of Eqs. (22) and (26) for the u_1^k and u_2^k terms present in Eqs. (19) and (20), respectively, to calculate the Kirchhoff diffraction contribution to the scattered field u_s^s over a larger angular domain about $\phi=\pi$. However, before the results of Eqs. (19) and (20) for $u_{s_h}^s$ can be

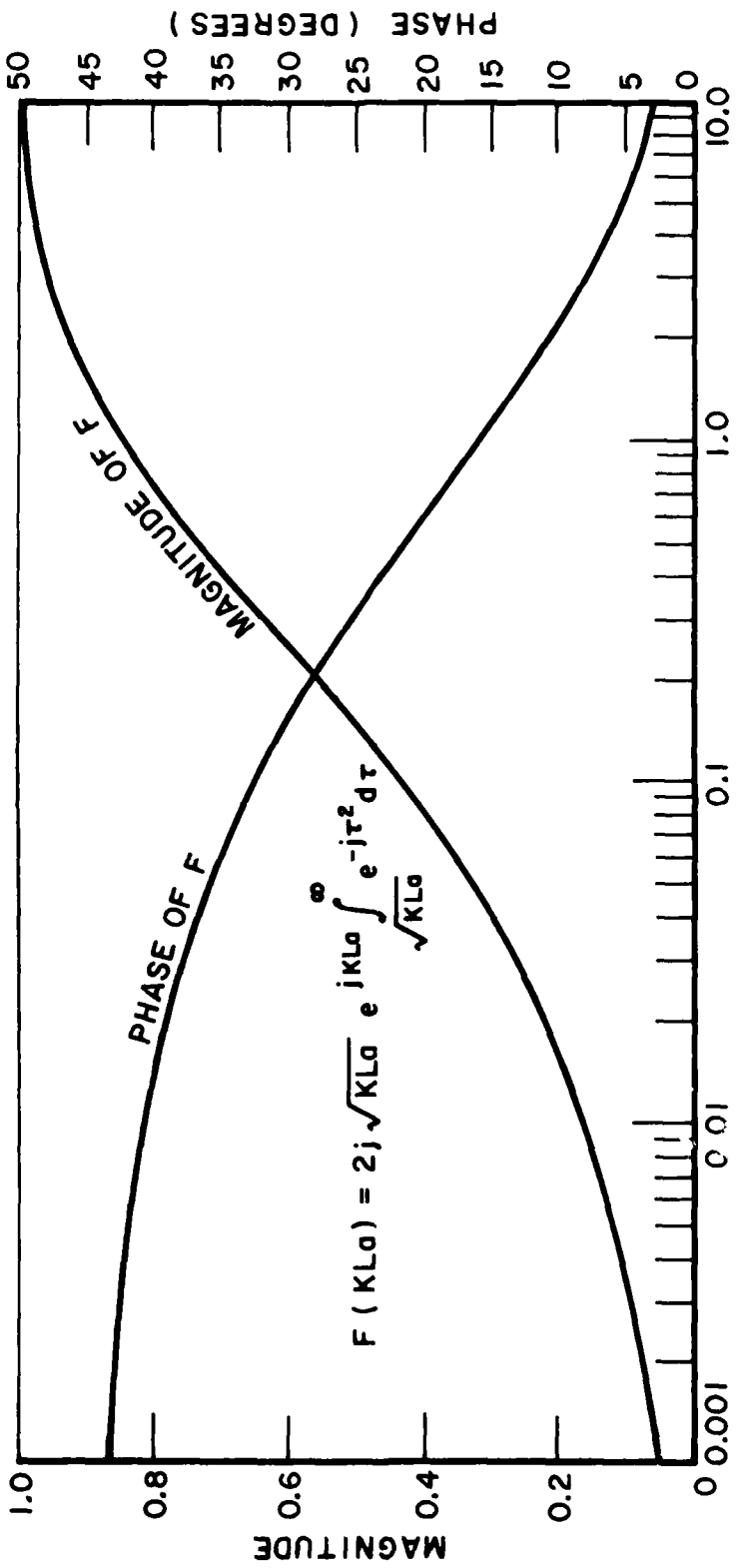

Fig. 6. A plot of F(X) vs X.

extended to calculate the scattered field over this larger angular domain about $\phi=\pi$, one must modify the terms involving $p^*(\xi)$ and $q^*(\xi)$ (which are viewed as corrections to Kirchhoff diffraction) in a manner corresponding to that employed for u_1^k in Eqs. (22) and (26). From Eqs. (A-10) and (A-24) of Appendix I:

$$(27a) \qquad \tilde{F}(\xi) = \frac{1}{\sqrt{\pi}} \int_{\Gamma_1} e^{-i\xi\tau} \frac{QV(\tau)}{QW_2(\tau)}\, d\tau + \frac{1}{2\sqrt{\pi}\xi} \quad ,$$

where

$$(27b) \qquad \tilde{F}(\xi) = \begin{cases} p^*(\xi) & \text{if the operator } Q = 1 \\ q^*(\xi) & \text{if the operator } Q = \frac{\partial}{\partial\tau} \end{cases}$$

and $\xi = \xi_1$ or ξ_2. The function $QV(\tau)$ is directly related to the Miller type Airy function as described in Appendix I. Clearly, the Kirchhoff correction terms in Eqs. (19) and (20) may be expressed in terms of $\tilde{F}(\xi)$ in Eqs. (27a) and (27b) as:

$$(28a) \qquad - e^{-i\pi/4} \sqrt{\frac{2}{k}} \left(\frac{ka}{2}\right)^{1/3} \tilde{F}(\xi)\, e^{-ika\psi} \frac{e^{-ik\rho}}{\sqrt{\rho}} =$$

$$= - e^{-i\pi/4} \sqrt{\frac{2}{k}} \left(\frac{ka}{2}\right)^{1/3} e^{-ika\psi} \frac{e^{-ik\rho}}{\sqrt{\rho}} \cdot \frac{1}{\sqrt{\pi}} \int_{\Gamma_1} e^{-i\xi\tau} \frac{QV(\tau)}{QW_2(\tau)}\, d\tau -$$

$$- (\text{unbounded Kirchhoff result of Eq. (21) for } \phi\tilde{\approx}_\pi),$$

with $\xi = \xi_1$ corresponding to $\psi = \psi_1$, as before. The unbounded Kirchhoff result for $\phi\tilde{\approx}_\pi$ is seen from Eq. (21) to be:

$$(28b) \qquad \pm \frac{e^{\mp ika(\phi-\pi)}}{(\phi-\pi)} \cdot \sqrt{\frac{1}{2\pi k}}\, e^{-i\pi/4} \frac{e^{-ik\rho}}{\sqrt{\rho}} .$$

The integral over the contour Γ_1 in Eq. (27a) is unbounded at $\xi=0$ (which corresponds to the shadow boundary at $\phi=\pi$), but $\tilde{F}(\xi)$ in Eqs. (27a) and (27b) (and therefore the result in Eq. (28a)) is bounded[4,7] because the

singularity in the $\frac{1}{2\sqrt{\pi\xi}}$ term of Eq. (27a) exactly cancels the singularity in the integral (over Γ_1) when $\xi \to 0$. It is then obvious that the Kirchhoff correction terms in Eqs. (19) and (20) can be appropriately modified to be useful over a larger angular domain about the shadow boundary ($\phi=\pi$), if the unbounded Kirchhoff result for ϕ in the close vicinity of π in Eq. (28a) is replaced by the unbounded Kirchhoff result valid over a larger angular domain about $\phi=\pi$. This is accomplished by noting from Eq. (22) that the factor $F(X)$ keeps $D_k(\phi)$ bounded at $\phi=\pi$, and:

$$\begin{pmatrix}\text{bounded Kirchhoff}\\ \text{diffraction field}\end{pmatrix} = \begin{pmatrix}\text{unbounded Kirchhoff}\\ \text{diffraction field}\end{pmatrix} \times F(X).$$

Thus, Eq. (28a) which is valid for $\phi \tilde{>} \pi$ is now modified by replacing

$$- e^{-i\pi/4} \sqrt{\frac{2}{k}} \left(\frac{ka}{2}\right)^{1/3} \tilde{F}(\xi_1) \, e^{-ika\psi_1} \frac{e^{-ik\rho}}{\sqrt{\rho}} \,,$$

with

$$(28c) \qquad - e^{-i\pi/4} \sqrt{\frac{2}{k}} \left(\frac{ka}{2}\right)^{1/3} e^{-ika\psi_1} \frac{e^{-ik\rho}}{\sqrt{\rho}} \left[\tilde{F}(\xi_1) - \frac{1}{2\sqrt{\pi}\xi_1}\right]$$

$$+ \sqrt{\frac{1}{2\pi k}} \, e^{-i\pi/4} \, \frac{\pm 1}{\sin\phi} \, \frac{e^{-ik(\rho \mp a\sin\phi)}}{\sqrt{\rho}} \,.$$

Combining the Kirchhoff diffraction results of Eq. (22) and Eq. (26) with the Kirchhoff correction terms of Eq. (28c) yield an expression for $u_s^s(P)$ which is useful over a larger angular domain about $\phi=\pi$ (in contrast to u_s^h Eq. (19) and Eq. (20) which are good only in the close vicinity of $\phi=\pi$):

$$(29a)\qquad u^s(P,P_{1,2}) \sim -\left(\sqrt{\frac{1}{2\pi k}}\cdot\frac{e^{-i\pi/4}}{\pm\sin\varphi}\,[F(X_{1,2})-1]\,\frac{e^{-ik(\rho\mp a\sin\phi)}}{\sqrt{\rho}}\right)$$

$$-\left(\sqrt{\frac{2}{k}}\left(\frac{ka}{2}\right)^{1/3} e^{-ika\psi_{1,2}} e^{-i\pi/4}\cdot\left[\tilde{F}(\xi_{1,2}) - \frac{1}{2\sqrt{\pi}\xi_{1,2}}\right]\frac{e^{-iks}}{\sqrt{s}}\right),$$

with $\quad X_1 = 2k\rho\cos^2\phi/2, \quad$ and $\quad X_2 = 2k\rho\cos^2(2\pi-\phi)/2.$

$u^s(P,P_{1,2})$ corresponds to the scattered field at P arising from the penumbral region associated with P_1 or P_2. Also

$$(29b)\qquad u^s(P,P_{1,2}) = \begin{cases} u_s^s(P,P_{1,2}), & \text{when } \tilde{F}(\xi_{1,2}) = P^*(\xi_{1,2}), \quad \text{for the } TM_z \text{ case} \\ u_h^s(P,P_{1,2}), & \text{when } \tilde{F}(\xi_{1,2}) = q^*(\xi_{1,2}), \quad \text{for the } TE_z \text{ case.} \end{cases}$$

The total h.f. field at a point P arising from the vicinity of P_1 on the cylinder may be written as:

$$(30a)\qquad u_s(P,P_1) \sim \begin{cases} u_s^i(P) + u_s^s(P,P_1) & \text{on the lit side } (\phi<\pi) \\ u_s^s(P,P_1) & \text{on the shadow side } (\phi>\pi) \end{cases}$$

for the TM_z case,

and

$$(30b)\qquad u_h(P,P_1) \sim \begin{cases} u_h^i(P) + u_h^s(P,P_1) & \text{on the lit side } (\phi<\pi) \\ u_h^s(P,P_1) & \text{on the shadow side } (\phi>\pi) \end{cases}$$

for the TE_z case.

The total h.f. field at P arising from the vicinity of P_2 on the cylinder is similarly expressed as:

(30c) $$u_s(P,P_2) \sim \begin{cases} u_s^i(P) + u_s^s(P,P_2) & \text{on the lit side } (\phi<\pi) \\ u_s^s(P,P_2) & \text{on the shadow side } (\phi>\pi) \end{cases}$$

for the TM_z case,

and

(30d) $$u_h(P,P_2) \sim \begin{cases} u_h^i(P) + u_h^s(P,P_2) & \text{on the lit side } (\phi<\pi) \\ u_h^s(P,P_2) & \text{on the shadow side } (\phi>\pi). \end{cases}$$

for the TE_z case.

The total h.f. field at P in the transition region is the sum of the fields arising from the vicinity of P_1 and P_2 on the cylinder, thus:

(31a) $$u_s(P) = u_s(P,P_1) + u_s(P,P_2) \qquad \text{for the } TM_z \text{ case}$$

and

(31b) $$u_h(P) = u_h(P,P_1) + u_h(P,P_2) \qquad \text{for the } TE_z \text{ case.}$$

The results of Eqs. (31a) and (31b) will be employed in part B which follows, to calculate the fields in the transition region associated with the canonical problem of Fig. 2. One notes that the results in Eqs. (29a) and (29b) are based on a direct generalization of the results in Eqs. (19) and (20). The accuracy of these results will be indicated in the next section wherein they are applied to specific problems. Possibly, a more accurate asymptotic h.f. result for $u^s(P,P_{1_2})$ (when P is not necessarily in the close vicinity of $\phi=\pi$ shadow boundary) obtained from first principles might involve terms that are not a simple superposition of the effective edge diffracted field term, and a surface dependent field term as in Eq. (29a); such an asymptotic solution based on mathematical rigor rather than on simplifying physical assumptions to bypass mathematical complexities appears to be a difficult task. However, judging from the

numerical results obtained from the use of Eq. (29a) in the following sections, it appears that the present solution yields sufficiently accurate values for engineering applications.

B. H.F. Scattering by a Perfectly-Conducting 2-D, Rounded-End Thick-Screen

The canonical configuration of interest is illustrated in Fig. 2. It is desired to calculate the total h.f. field surrounding this 2-D rounded-end, thick-screen configuration when it is excited by a normally incident electromagnetic plane wave of the TM_z or the TE_z type. The solution to this canonical problem is of relevance to a study of the effects of the aircraft fuselage on the radiation from wing mounted antennas, as indicated previously. Figure 2 illustrates the junctions J_1 and J_2 resulting from the smooth join of the half-cylinder onto the thick half plane. In the present analysis, the diffraction effects arising from the junctions J_1 and J_2 are not included for the following reasons:

1) The actual fuselage of an aircraft will be approximated by this model for which these junctions will only be artificially added to our model in that they are not present in the actual aircraft structure.

2) The junction effects are important only if the penumbral region lies in the neighborhood of the junction, or if the field point lies in the neighborhood of the reflection boundary associated with the junction. It is clear therefore, that in the present problem, which deals with normal incidence and with aspects within and near the transition region, the junction effects are negligible.

The total h.f. field in the lit region for the problem in Fig. 2 is adequately described by the fields associated with the incident and reflected rays of geometrical optics, whereas, the h.f. field in the shadow

region is accurately described by the surface diffracted rays of Keller's geometrical theory of diffraction[9] (hence by the GTD). However, the geometrical optics field description fails near and on the reflection boundary (which is also the shadow boundary in this case). On the other hand the GTD field description requires an increasing number of surface ray modes to accurately describe the field near the shadow boundary thereby making the GTD result cumbersome to employ. Thus, within and near the transition region adjacent to the shadow boundary, one may employ the result developed in part A to calculate the total h.f. fields there. The specific results for the lit, transition, and shadow regions associated with the canonical configuration of Fig. 2 are indicated below.

Field Description in the Lit Region - The total field in the lit region is a superposition of the incident field u^i, and the reflected field u^r predicted by geometrical optics, in which

$$u^i = u^i_{\substack{s \\ h}} = e^{ikx}, \qquad \text{for } \begin{matrix} TM_z \\ TE_z \end{matrix} \text{ case,} \tag{32a}$$

and,

$$u^r = u^r_{\substack{s \\ h}} = u^i_{\substack{s \\ h}}(P_R) \cdot R_{\substack{s \\ h}} \sqrt{\frac{\rho_r}{\rho_r + s}}\; e^{-iks} \tag{32b}$$

where the subscript s is used for the TM_z case, and the subscript h is used for the TE_z case as before. The result in Eq. (32b) is in a ray-optical form[11] which is valid in the near zone. P_R denotes the point of reflection in Fig. 7a, and $u^i_{\substack{s \\ h}}(P_R)$ is the value of the incident $\left(\begin{matrix} TM_z \\ TE_z \end{matrix}\right)$ field at P_R. The reflection coefficient, $R_{\substack{s \\ h}}$ is defined by:

$$R_s = -1, \qquad \text{for the } TM_z \text{ case,} \tag{32c}$$

$$R_h = +1, \qquad \text{for the } TE_z \text{ case.} \tag{32d}$$

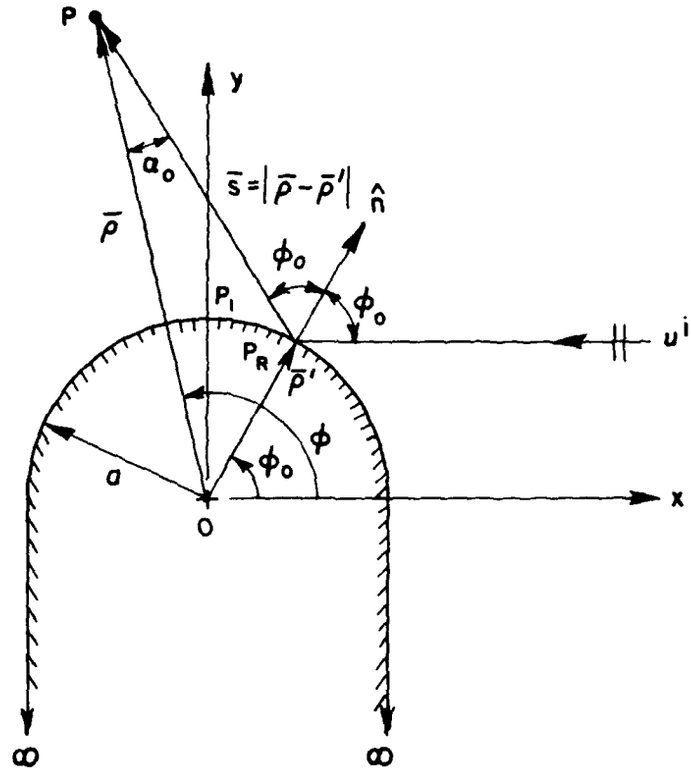

Fig. 7a. Reflected ray geometry.

s denotes the distance from P_R to the field point P in the lit zone. The quantity ρ_r within the radical in Eq. (32b) refers to the caustic distance (in the plane of reflection) associated with the reflected wavefront; ρ_r is found to be:

$$\rho_r = \frac{a\cos\phi_o}{2} \quad . \tag{32e}$$

The total field at a point P in the lit zone is thus given by:

$$u_{s_h}(P) \sim u^i_{s_h}(P) + u^i_{s_h}(P_R)\,(\mp 1)\,\sqrt{\frac{a\cos\phi_o}{a\cos\phi_o + 2s}}\; e^{-iks}; \quad \text{for } \begin{matrix} TM_z \\ TE_z \end{matrix} \text{ case.} \tag{32f}$$

If far zone results are desired, one must enforce the condition $s >> \rho_r$ in Eq. (32b). The result in Eq. (32f) is valid in the lit zone for aspects sufficiently far from the reflection boundary (which occurs when P_R coincides with P_1).

Field Description in the Transition Region - The total field in the transition region may be immediately written down from Eqs. (30a) and (30b) given in Part A. It is conjectured here that the fields in the transition region of Fig. 2 are identical to those in Eqs. (30a) and (30b) which arise from the penumbral region associated with P_1 on the circular cylinder of Fig. 1. This conjecture is based on the h.f. approximation which allows one to consider h.f. diffraction as being a local phenomenon. The results in Eqs. (30a) and (30b) for the TM_z and the TE_z cases, respectively, are valid in the far zone; however, since h.f. diffraction is a local phenomenon, one may also directly modify the far-zone results of Eqs. (30a) and (30b) to obtain the following near zone transition fields at P:

$$(33) \qquad \underset{h}{u_s}(P) \sim \underset{h}{u_s^i}(P) \cdot H(\pi-\alpha) + \left\{ -\left(\sqrt{\frac{1}{2\pi k}}\, e^{-i\pi/4}\, \frac{[F(X)-1]}{\sin\alpha}\, \frac{e^{-ikd}}{\sqrt{d}} \right) - \left(\sqrt{\frac{2}{k}} \left(\frac{ka}{2}\right)^{1/3} \cdot \right.\right.$$

$$\left.\left. \cdot\, \tilde{e}^{ika\psi}\, e^{-i\pi/4} \left[\tilde{F}(\xi) - \frac{1}{2\sqrt{\pi}\xi} \right] \frac{e^{-iks}}{\sqrt{s}} \right) \right\}$$

with the understanding that $\tilde{F}(\xi) = P^*(\xi)$ for $u_s(P)$ and $\tilde{F}(\xi) = q^*(\xi)$ for $u_h(P)$; also $H(\pi-\alpha)$ is the Heaviside step function whose value is unity if $\alpha<\pi$ and zero if $\alpha>\pi$. The near zone result of Eq. (33) is obtained by simply replacing the far zone ray distances by their corresponding near zone ray distances. The quantities s, ψ and ξ in Eq. (33) are given in terms of the near field coordinates by:

$$(34a) \qquad s = \begin{cases} s_\ell & \text{in the lit portion of the transition region} \\ s_s & \text{in the shadowed portion of the transition region} \end{cases}$$

(34b),(34c) $\xi = \left(\frac{ka}{2}\right)^{1/3} \psi$; $\psi \equiv \begin{cases} -|\psi_\ell|, & \text{in the lit portion of the transition region.} \\ |\psi_s|, & \text{in the shadowed part of the transition region.} \end{cases}$

where the angles ψ_ℓ and ψ_s, and the distances s_ℓ and s_s are indicated in Fig. 7b below. The F(X) function appearing in Eq. (33) is defined earlier

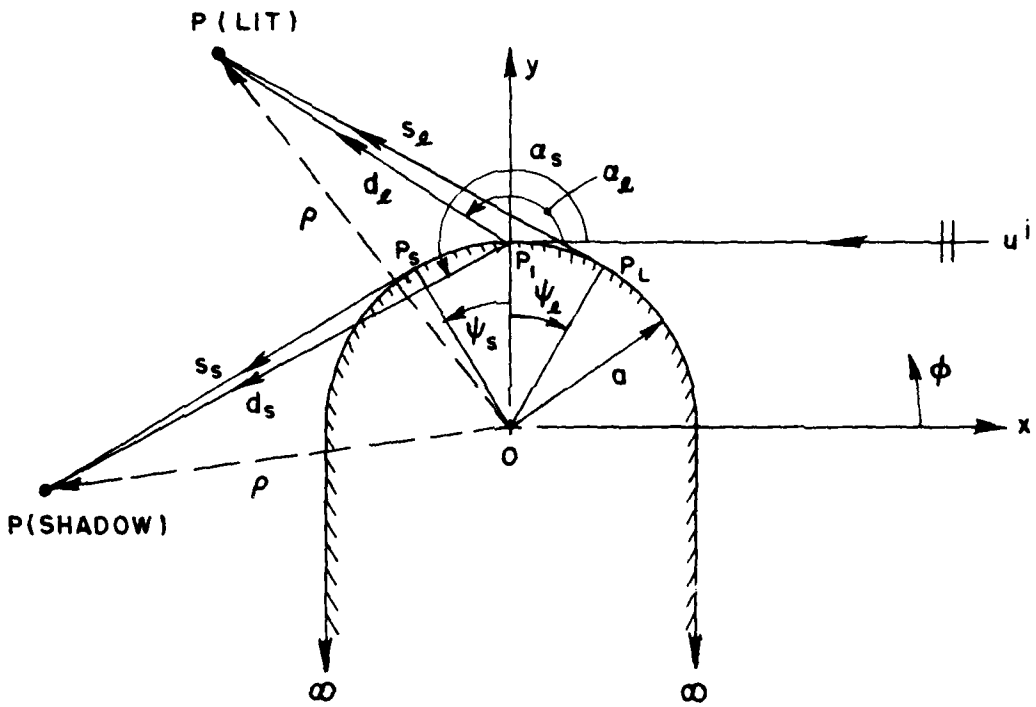

Fig. 7b. Equivalent ray geometries for the fields in the lit and shadowed portions of the transition region associated with the shadow boundary at P_1.

in Eq. (24a). The new argument (for near zone calculations) of F(X) is clearly:

(35a) $X = 2kd \cos^2 \frac{\alpha}{2}$

where α is the angle (measured in the cw sense) subtended by the Kirchhoff diffracted ray (directed along $\overline{P_1P}$) and the negative of the incident ray direction (i.e., along + x).

$$\alpha = \begin{cases} \alpha_\ell & \text{in the lit part} \\ \alpha_s & \text{in the shadowed part.} \end{cases} \tag{35b}$$

The distance d is measured from P_1 to P and

$$d = \begin{cases} d_\ell & \text{in the lit part} \\ d_s & \text{in the shadowed part.} \end{cases} \tag{35c}$$

The quantities α_ℓ, α_s, d_ℓ and d_s are illustrated in Fig. 7b.

The transition region solution discussed above must serve a two-fold objective, namely that it should provide a sufficiently accurate h.f. field description within the transition region; secondly, it should blend smoothly with the geometrical optics solution in the lit region, and also blend smoothly with the GTD solution in the shadow region. Some numerical calculations which indicate the accuracy of the present results are provided later.

Field Description in the Shadow Region - For aspects in the deep shadow region, the scattered field (the incident field is zero within the shadow region) is given a ray optical representation valid in the near zone. The result based on GTD is given as[11]:

$$u_{s\,h}(P) \sim u^{s}_{s\,h}(P) = \sum_{p=1}^{\infty} u^{i}_{s\,h}(P_1) \cdot D^{s}_{h\,p}(P_1)\, e^{-\alpha^{s}_{h\,p} a\psi_s - ika\psi_s}\, D^{s}_{h\,p}(P_D)\, \frac{e^{-iks}}{\sqrt{s}} \tag{36}$$

$$= \sum_{p=1}^{\infty} D^{s}_{h\,p}(P_1)\, e^{-\alpha^{s}_{h\,p} a\psi_s - ika\psi_s}\, D^{s}_{h\,p}(P_D)\, \frac{e^{-iks}}{\sqrt{s}}, \quad \text{for } \begin{matrix} TM_z \\ TE_z \end{matrix} \text{ case,}$$

since $u_{s,h}^{i}(P_1) = 1$. The geometrical details are given in Fig. 7c for the

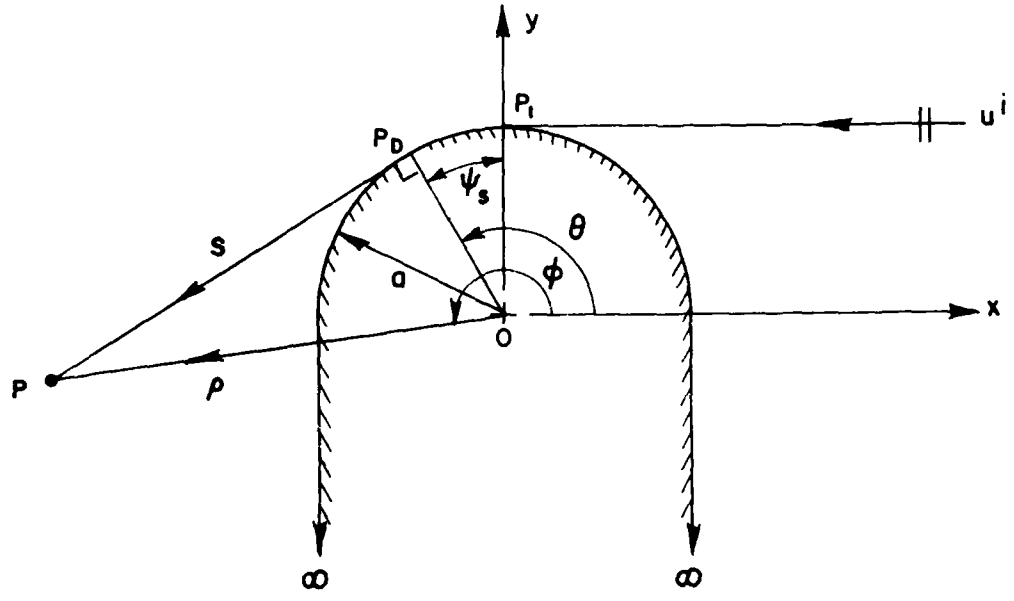

Fig. 7c. Ray geometry for the GTD fields.

surface ray modes which traverse a path P_1P_DP to the field point. Even though the inclusion of an infinite number of GTD surface ray modes is indicated in Eq. (36), it is generally found that sufficiently accurate results for the field are obtained by summing only the first five modes (corresponding to p=1 to p=5), provided the field point P is far-removed from the transition region. $D_p^{s,h}$ and $\alpha_p^{s,h}$ are the cylinder diffraction coefficient and attenuation constant for the p-th surface ray mode, respectively. D.R. Voltmer (in his Ph.D dissertation, Ohio State University, 1970) has obtained diffraction coefficients and attenuation constants to order $(\frac{2}{k\rho_g})^{2/3}$ (here ρ_g = local radius of curvature of the surface along the ray path) which are valid for smooth convex surfaces of non-constant curvature (this includes the circular cylinder, and the sphere as special cases); a

table of his diffraction coefficients and attenuation constants is, also, available in Reference [8]. The superscripts s and h on the diffraction coefficient and attenuation constant denote the TM_z and the TE_z cases, respectively.

Numerical Results - The numerical results for the near field patterns of a circular cylindrically tipped thick half plane (as shown in Fig. 2) illuminated by a TM_z (acoustic soft) or TE_z (acoustic hard) plane wave have been calculated via the formulas developed above. These results are illustrated in Figs. 8 through 10. The geometrical optics field shown as a dot-dashed line, consists of the incident and reflected fields up to the shadow boundary. The transition field, shown as a solid line, starts at $\phi=90°$ and is shown into the deep shadow region. The surface ray mode field (obtained by summing over only the first 5 modes) is shown as a dotted line and is valid in the deep shadow region. Note that the geometrical optics field and the transition field blend well in the angular range $90°<\phi<120°$. The transition field and the surface ray mode field for the hard cases blend in the neighborhood of $\phi=180°$. The soft cases do not blend as quickly. The phase for the above near field patterns also blended well; however, it is difficult to illustrate and will not be shown here.

The validity of the above high frequency solutions is demonstrated by applying them to the problem of plane wave scattering by a circular cylinder (as shown in Fig. 1). The results are then compared with the exact solution for the problem which is found from the eigenfunction expansion in Figs. 11a and 11b. The high frequency solution is composed of the superposition of fields from the two penumbral regions associated with P_1 and P_2 using the appropriate results (of part B) in their respective regions of validity. The good agreement lends confidence to the present high frequency solutions.

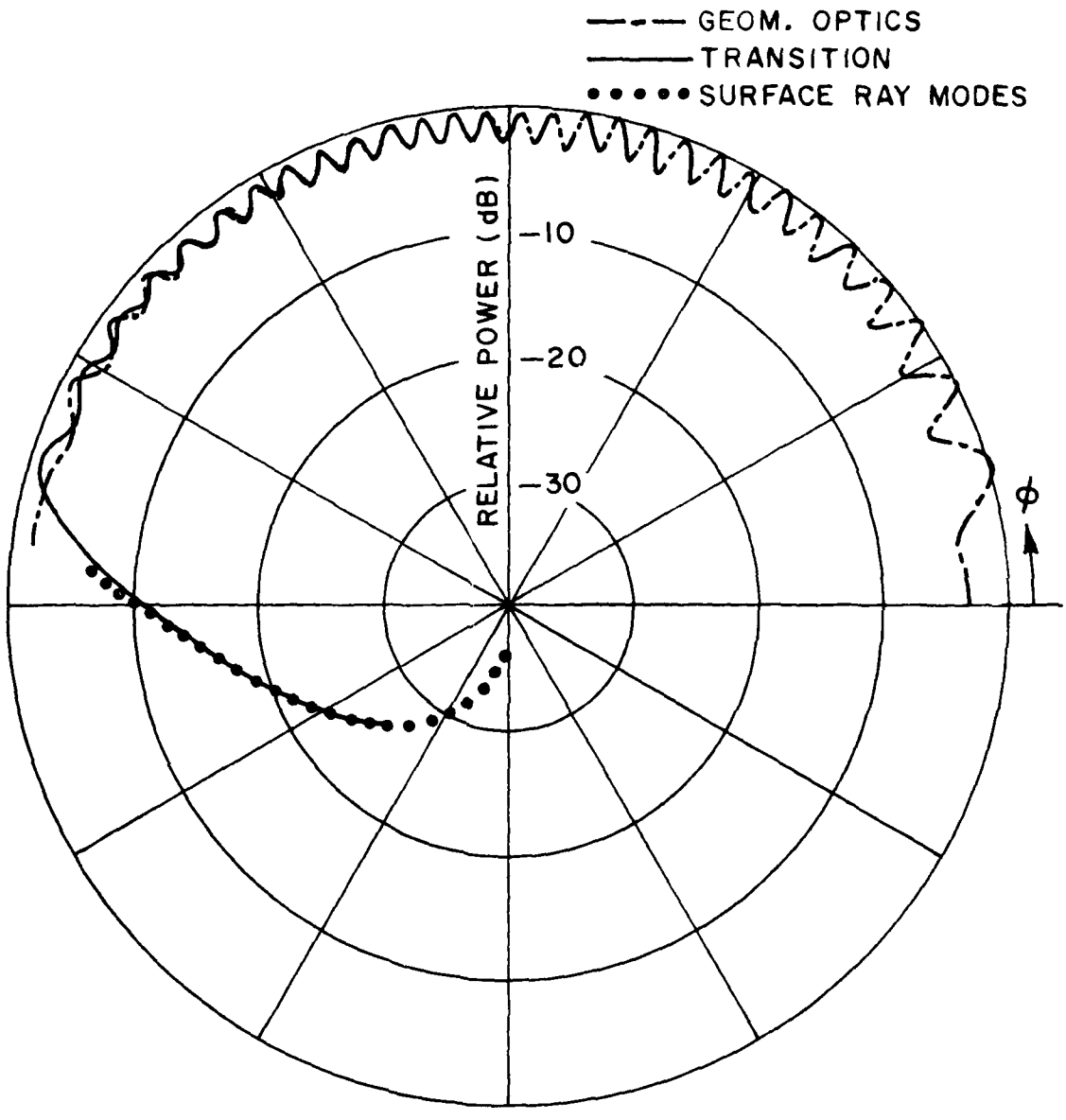

Fig. 8a. Near field pattern for cylindrically tipped thick half-plane, hard case, ka=10, kρ=100.

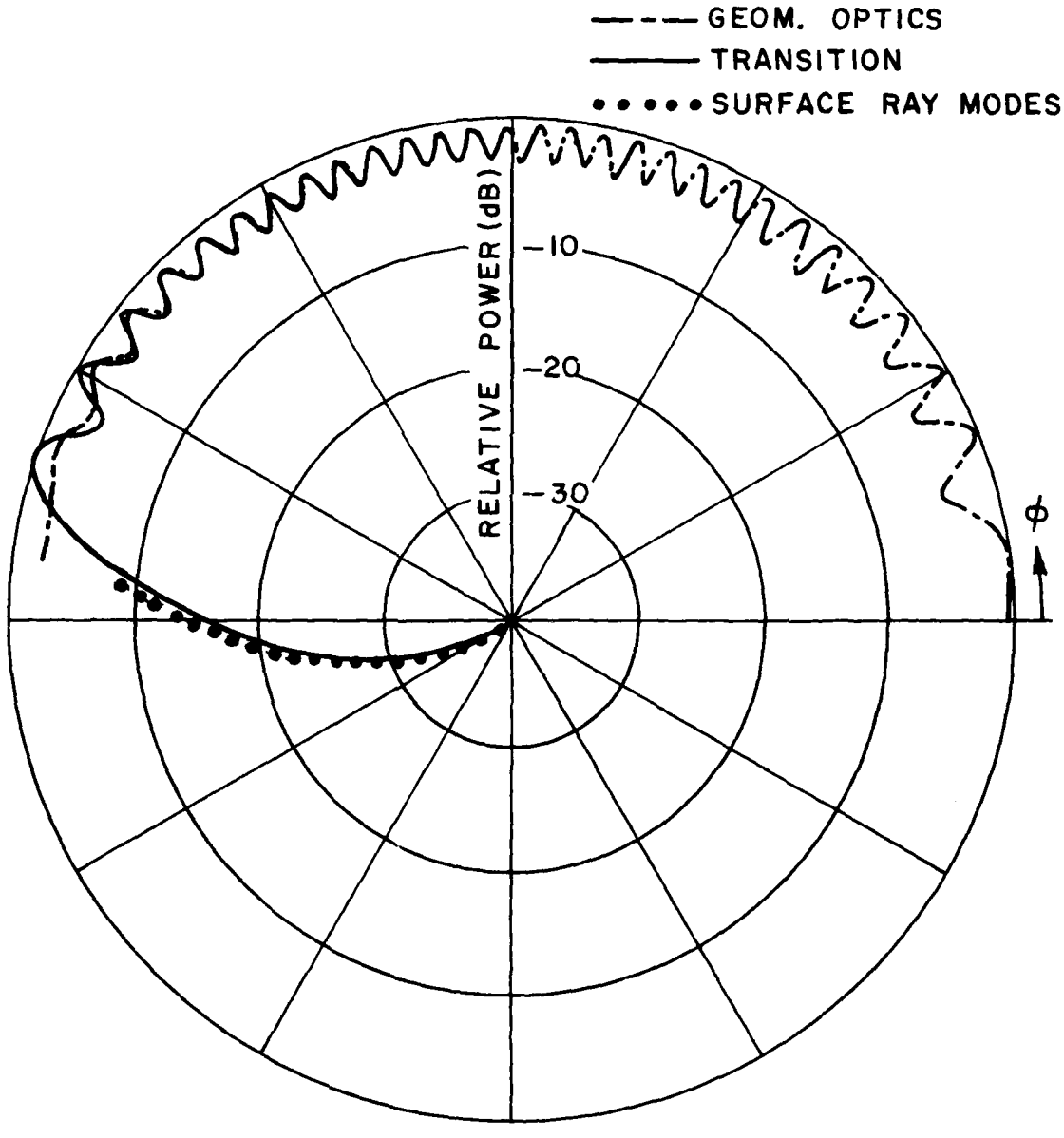

Fig. 8b. Near field pattern for cylindrically tipped thick half-plane, soft case, ka=10, kρ=100.

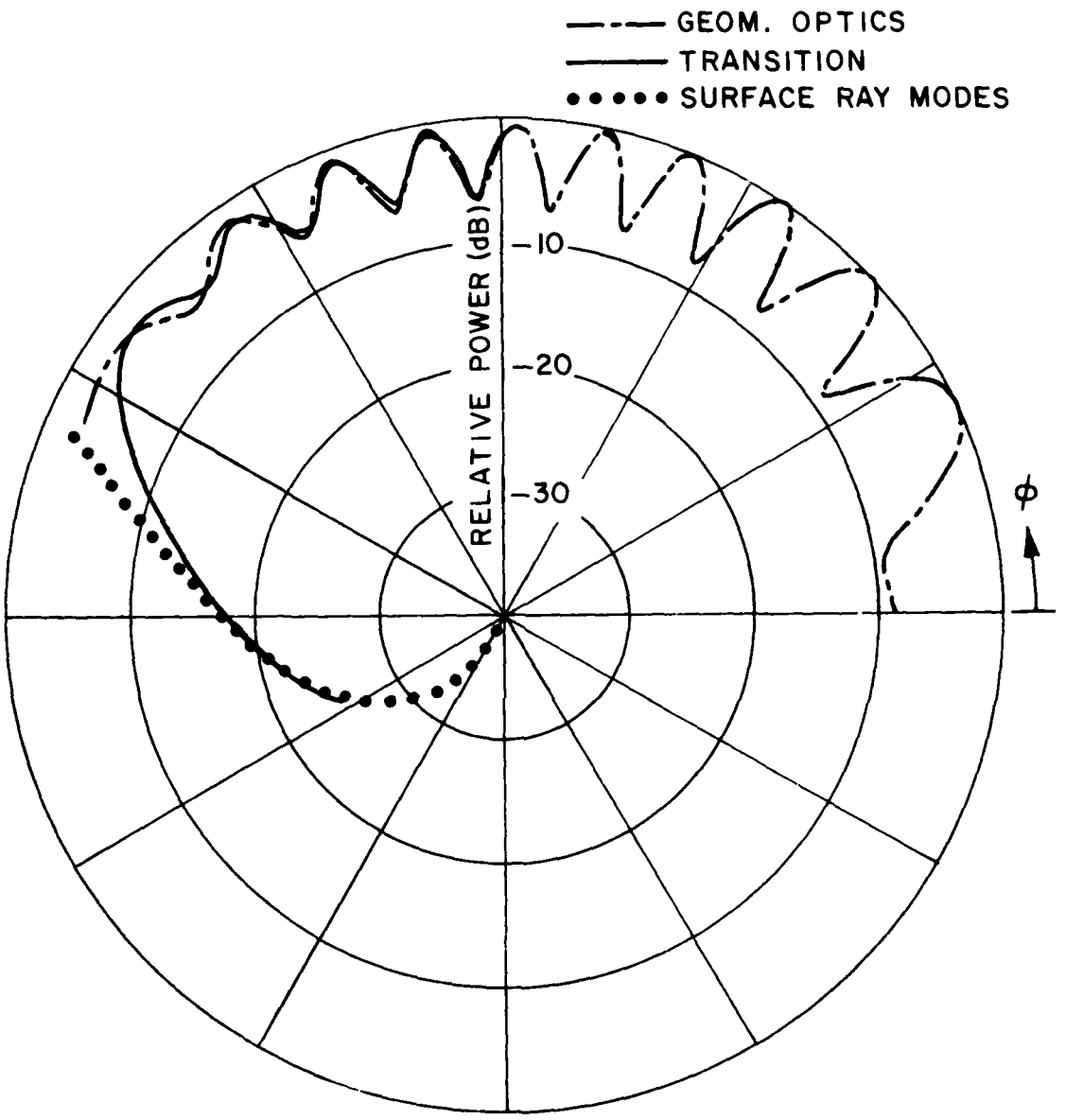

Fig. 9a. Near field pattern for cylindrically tipped thick half-plane, hard case, ka=20, kρ=50.

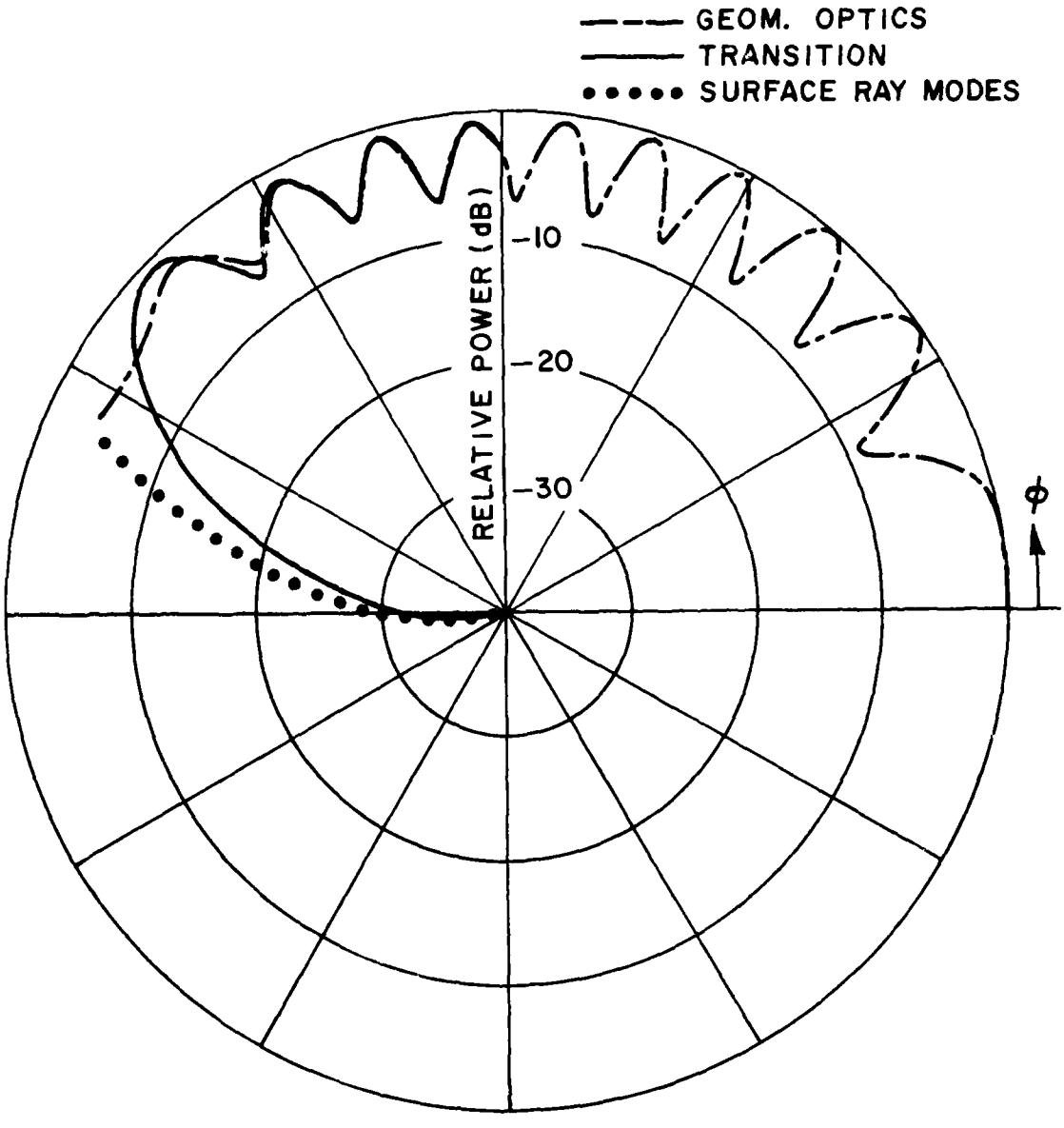

Fig. 9b. Near field pattern for cylindrically tipped thick half-plane, soft case, ka=20, kρ=50.

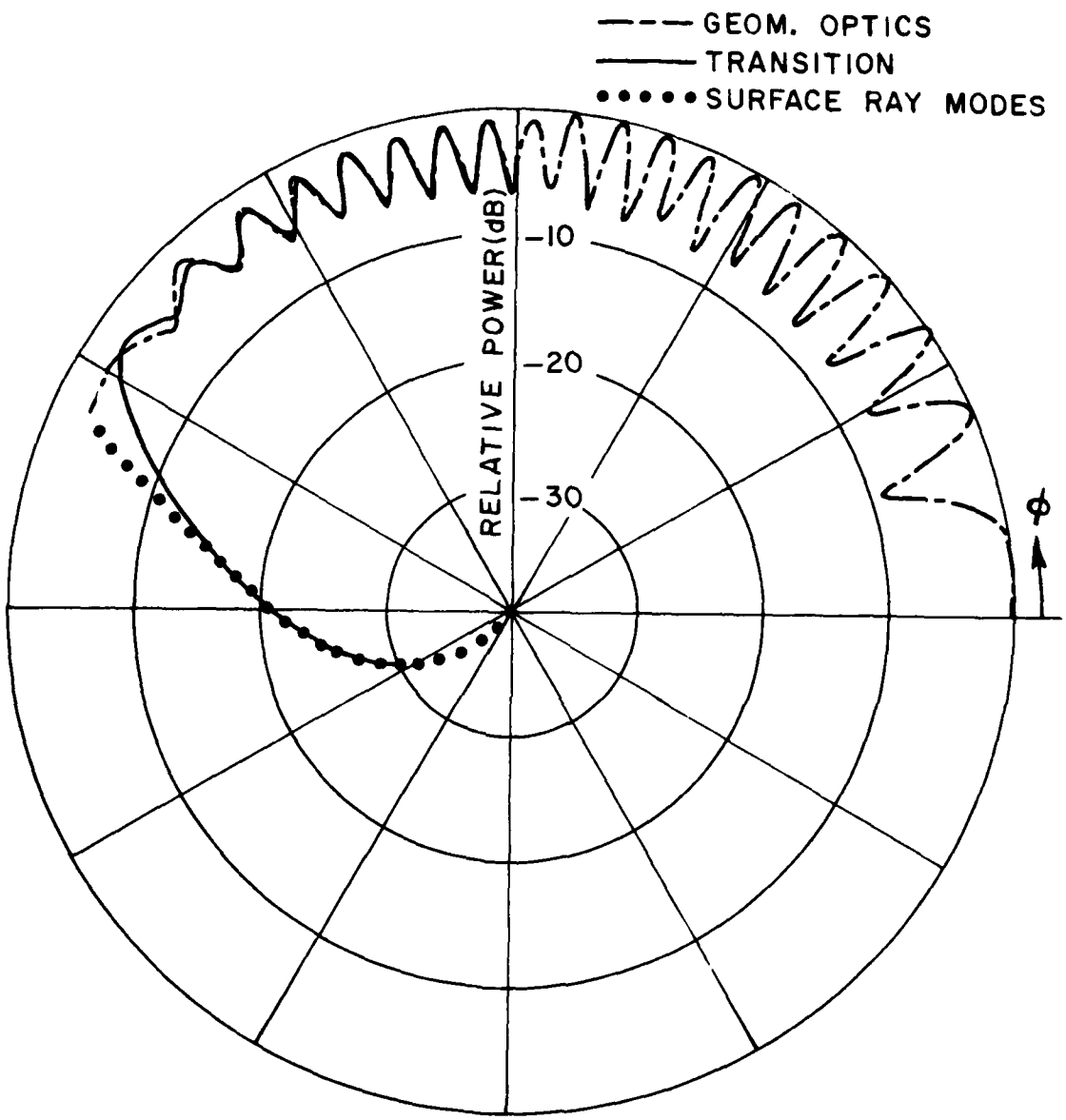

Fig. 10a. Near field pattern for cylindrically tipped thick half-plane, hard case, ka=40, $k\rho$=100.

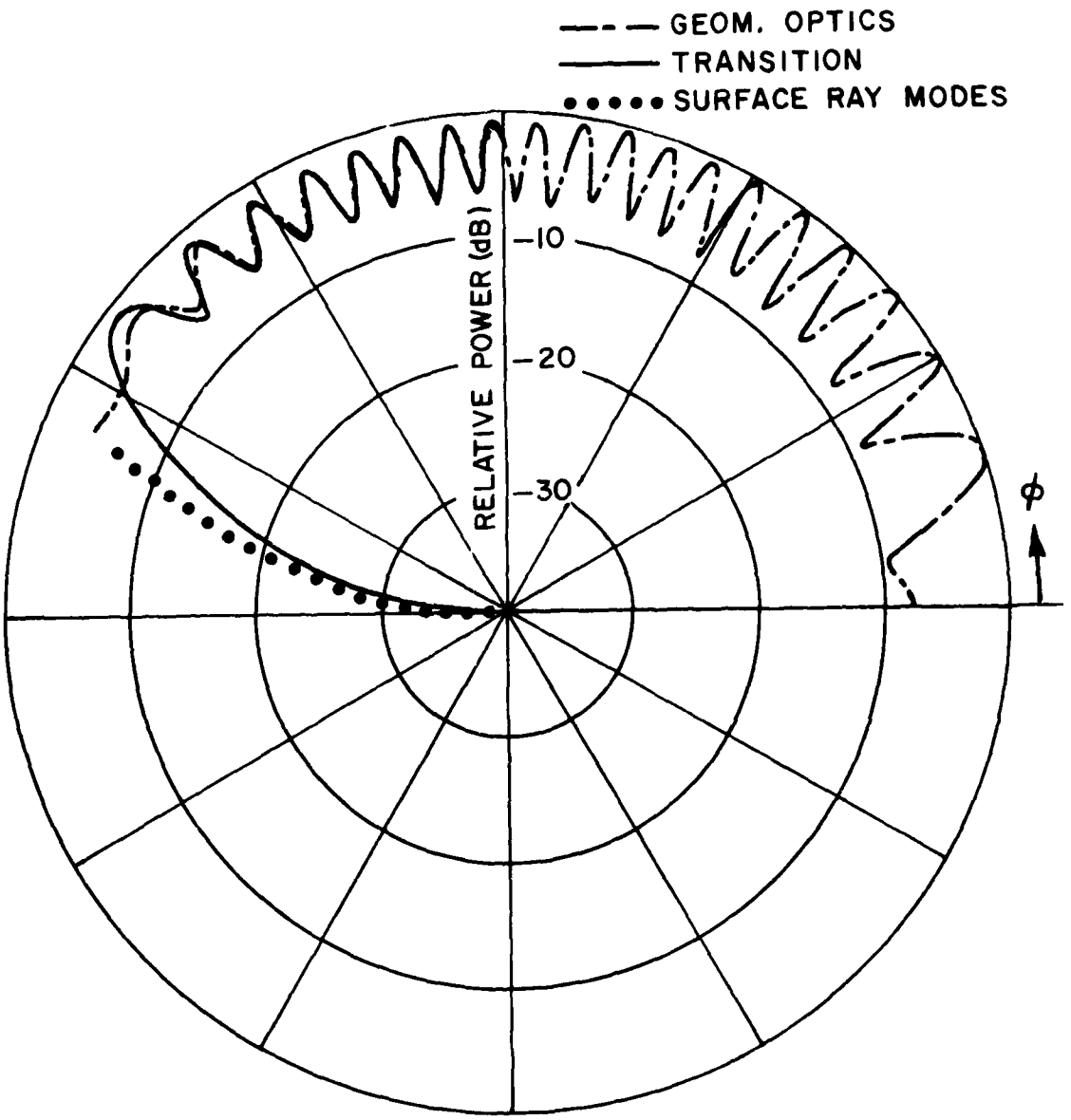

Fig. 10b. Near field pattern for cylindrically tipped thick half-plane, soft case, $ka=40$, $k\rho=100$.

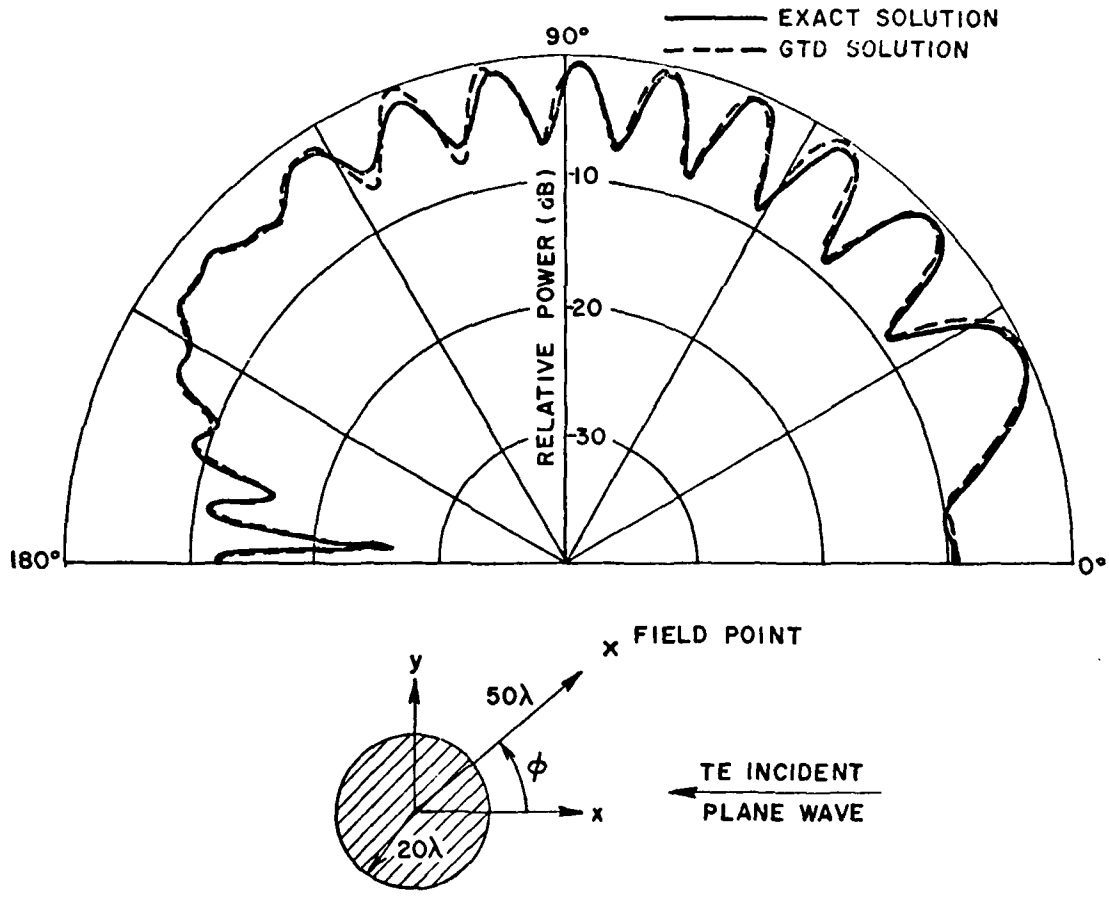

Fig. 11a. Comparison of high frequency solution with exact solution for near field pattern of circular cylinder, hard case, ka=20, $k\rho$=50.

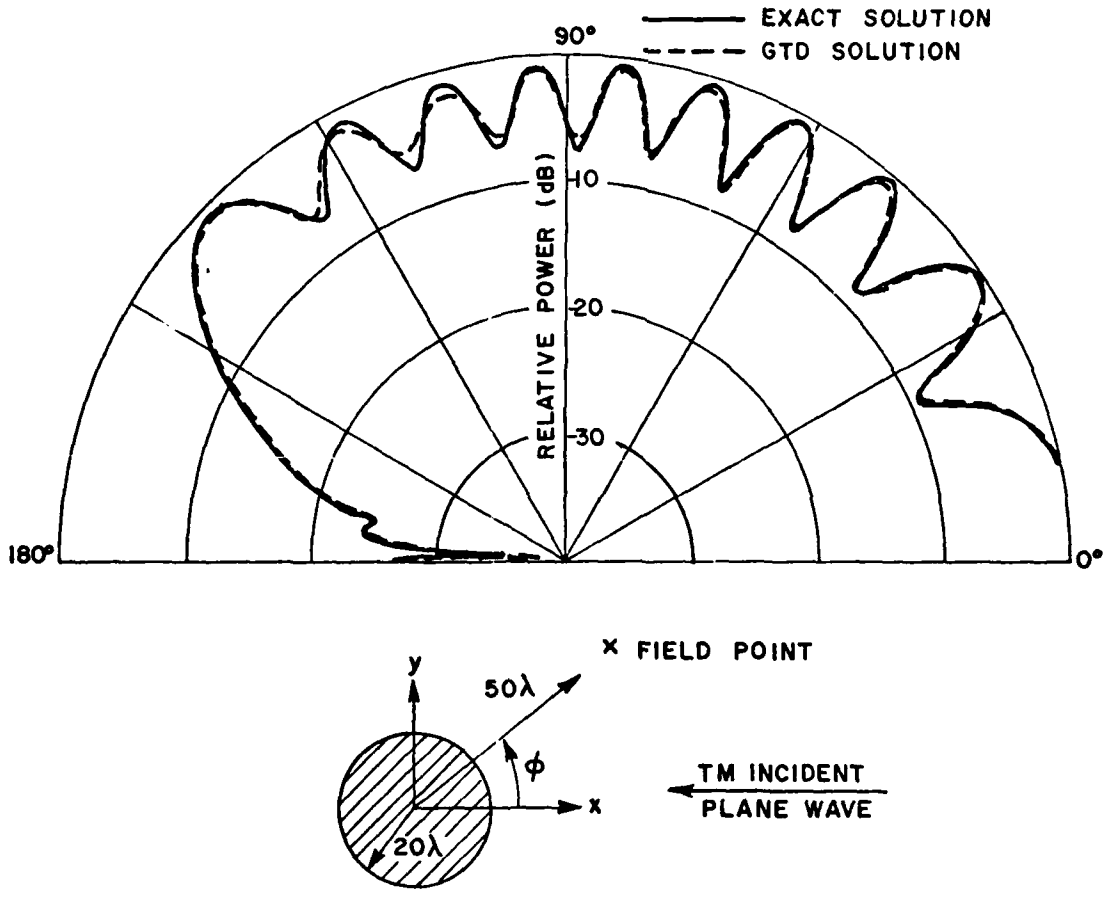

Fig. 11b. Comparison of high frequency solution with exact solution for near field pattern of circular cylinder, soft case, ka=20, kρ=50.

III. HIGH FREQUENCY SCATTERING BY A 3-D, SMOOTH CONVEX SURFACE

As developed in the previous section the transition solution can be divided into two terms. These are the Kirchhoff term, which is independent of the polarization and curved surface properties, and a second term which is dependent on the surface curvature and associated electrical properties. The usefullness of this solution is that each of these terms can be systematically modified to three-dimensional surfaces (based on the high frequency assumption that diffraction is a local phenomenon). One notes that the geometrical optics and geometrical theory of diffraction solutions are well-known for the three-dimensional case as presented in Reference [11].

In this section, the near zone scattering by a spherically capped semi-infinite circular cylinder when excited by a normally incident plane wave is examined as shown in Fig. 12. The object of this study is to illustrate the three-dimensional nature of our high frequency solution and to verify that it blends nicely with the geometrical optics field. The field surrounding the configuration in Fig. 12 is given below in the lit, transition, and shadow regions in a manner similar to that indicated for the canonical configuration of Fig. 2, in part B of the previous section. Once again, the diffraction effects arising from the junction of the hemispherical cap and the cylinder are ignored for reasons indicated previously.

Field Description in the Lit Region - The geometrical optics solution composed of the incident field (u^i) and the reflected field (u^r) observed at a near zone field point P in the lit zone is explicitly given by:

$$(37) \qquad u_{s_h}(P) \sim u^i_{s_h}(P) + u^i_{s_h}(P_R) \cdot R_{s_h} \sqrt{\frac{a^2 \cos\phi_o}{(a\cos\phi_o + 2s)(a + 2s\cos\phi_o)}}\, e^{-iks}; \quad \text{for } \begin{matrix} TM_z \\ TE_z \end{matrix} \text{ case.}$$

The point of reflection P_R and other geometrical parameters (such as a, s, ϕ_o, etc.) are the same as in Fig. 7a. The reflection coefficient R_{s_h} was

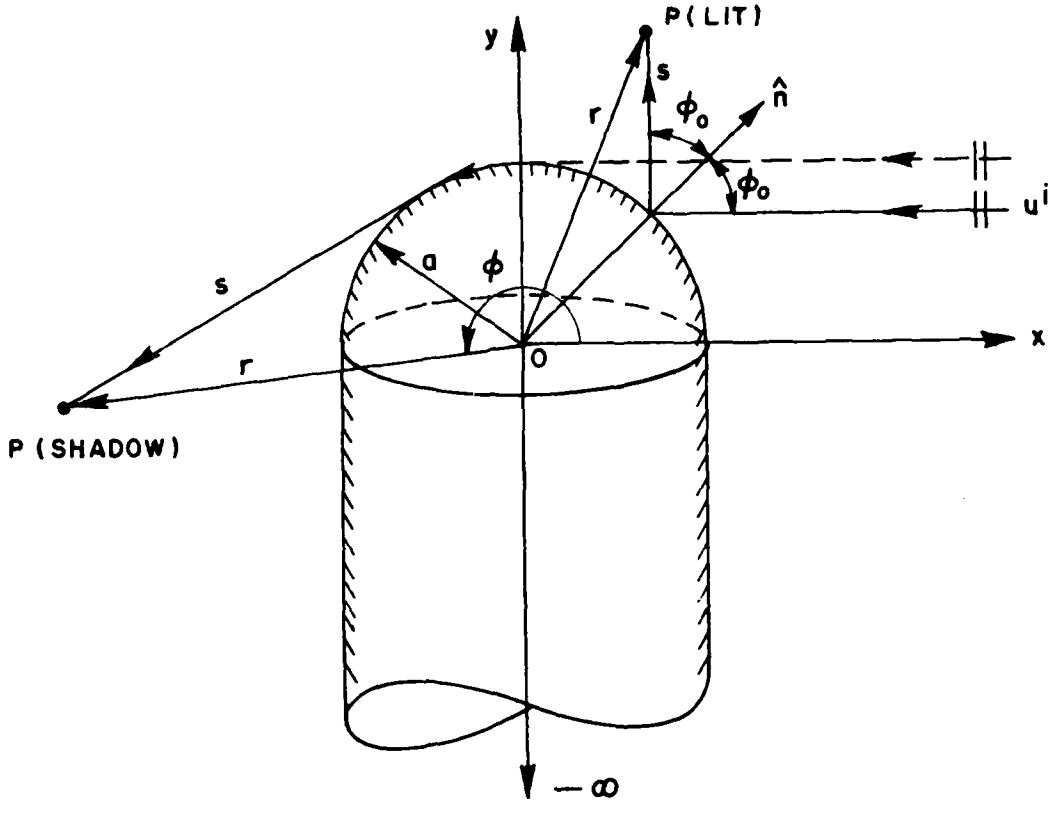

Fig. 12. Geometrical configuration for the hemispherically capped semi-infinite circular cylinder.

previously defined in Eqs. (32c) and (32d). $u_{s_h}^i(P_R)$ denotes the value of $u_{s_h}^i$ at the point of reflection P_R on the hemispherical cap.

Field Description in the Transition Region - The total field in the transition region for the 3-D geometry of Fig. 12 can be obtained by generalizing the 2-D results for the geometry in Fig. 2 which are indicated in Eq. (33). This generalization from 2-D to 3-D is based on the ray-optic description for the fields; analogous generalizations have been previously indicated elsewhere[8,9,11,12] for certain antenna and scattering problems. We obtain

$$(38a)\qquad u_s^h(P) \sim u_s^{i,h}(P)H(\pi-\alpha)+\left\{-\left(\sqrt{\frac{1}{2\pi k}}\, e^{-i\pi/4}\, \frac{[F(X)-1]}{\sin\alpha}\sqrt{\frac{a}{d(a+d\sin\alpha)}}\, e^{-ikd}\right)\right.$$
$$\left.-\left(\sqrt{\frac{2}{k}}\,\left(\frac{ka}{2}\right)^{1/3} e^{-ika\psi}\, e^{-i\pi/4}\left[\tilde{F}(\xi)-\frac{1}{2\sqrt{\pi}\xi}\right] e^{-iks}\, f(s)\right)\right\}$$

where $H(\pi-\alpha)$, $\tilde{F}(\xi)$, $F(X)$, α, s, d and ψ have the same meaning as in Eq. (33). The quantity $f(s)$ is given by:

$$(38b)\qquad f(s) = \begin{cases} \sqrt{\dfrac{\rho}{s(\rho+s)}} & \text{in the illuminated region } (\alpha<\pi) \\ \sqrt{\dfrac{d\eta_o}{d\eta}}\sqrt{\dfrac{\rho}{s(\rho+s)}} & \text{in the shadow region } (\alpha>\pi). \end{cases}$$

The geometrical details are the same as those indicated in Fig. 7b. The quantity $\sqrt{\frac{d\eta_o}{d\eta}}$ is the spatial spread of the field on the surface of the hemispherical cap along the ray path P_1P_s of Fig. 7b. In particular, $d\eta_o$ is the width of two adjacent rays at P_1; whereas, $d\eta$ is the width of the same two adjacent rays evaluated at P_s. The quantity $\sqrt{\frac{d\eta_o}{d\eta}}$ is given by:

$$(38c)\qquad \sqrt{\frac{d\eta_o}{d\eta}} = \sqrt{\frac{1}{\sin\theta}}$$

where $\theta = \begin{cases} \theta_{lit} & \text{in the lit penumbra region } (=\pi/2 - |\psi_\ell|) \text{ i.e., for } \theta<\frac{\pi}{2} \\ \theta_{sh} & \text{in the shadow penumbra region } (=\pi/2 + |\psi_s|) \text{ i.e., for } \theta>\frac{\pi}{2}. \end{cases}$

Also, the caustic distance ρ appearing in Eq. (38a) is the radius of curvature of the diffracted wavefront in the plane $\perp$ x-y plane, but containing the ray shed from the surface; it is given by

$$(38d)\qquad \rho = a\tan\theta.$$

Incorporating Eqs. (38c) and (38d) in $\sqrt{\frac{d\eta_o}{d\eta}}\ \sqrt{\frac{\rho}{s(\rho+s)}}$ of Eq. (38b) leads to

$$(38e) \qquad \sqrt{\frac{d\eta_o}{d\eta}}\sqrt{\frac{\rho}{s(\rho+s)}} = \sqrt{\frac{a}{s(a\sin\theta+s\cos\theta)}} \ .$$

Thus, $\rho>0$ when $\theta=\theta_{lit}$, whereas $\rho<0$ for $\theta=\theta_{sh}$. If

$$\frac{\rho}{s(\rho+s)} < 0,$$

then

$$\sqrt{\frac{\rho}{s(\rho+s)}} = \left|\sqrt{\frac{\rho}{s(\rho+s)}}\right| e^{i\pi/2}$$

because a caustic has been crossed. One notes that $\sqrt{\frac{d\eta_o}{d\eta}}$ has been replaced by unity in the lit part of the transition region (see Eq. (38b)) because it is conjectured that the fields scattered into the lit portion should be independent of the spatial spread factor of the rays along P_1P_L on the surface (this fact is directly evident in the reflected ray description for the lit region).

In order to keep the Kirchhoff diffracted term bounded one notes that the X in F(X) of Eq. (38a) should be

$$(38f) \qquad X = 2k\left[\frac{d(\rho_e+d)}{\rho_e}\right]\cos^2\alpha/2.$$

The quantity ρ_e is the caustic distance for the Kirchhoff diffracted ray in the plane containing the diffracted ray and the edge of the curved screen at P_1; it is computed easily via the formula for caustic distances for curved edges given by Kouyoumjian[12].

Field Description in the Shadow Region - The diffracted ray field within the shadow region at a field point P in the near zone is obtained by extending the 2-D result of Eq. (36) to the 3-D result in the usual manner[11].

$$(39)\quad u_{s}^{h}(P) \sim u_{s}^{s}(P) = \sum_{p=1}^{\infty} u_{s}^{i}(P_1)\cdot D_{p}^{s}(P_1)\, e^{-\alpha_{p}^{s}a\psi_s - ika\psi_s}\, D_{p}^{s}(P_D) \sqrt{\frac{d\eta_o}{d\eta}}\sqrt{\frac{\rho}{s(\rho+s)}}\, e^{-iks};$$

$$\text{for } \begin{matrix} TM_z \\ TE_z \end{matrix} \text{ case}$$

$$= \sum_{p=1}^{\infty} D_{p}^{s}(P_1)\, e^{-\alpha_{p}^{s}a\psi_s - ika\psi_s}\, D_{p}^{s}(P_D) \sqrt{\frac{a}{s(a\sin\theta+s\cos\theta)}}\, e^{-iks},$$

where $u_{s}^{i}(P_1) = 1,$

and $$\sqrt{\frac{d\eta_o}{d\eta}}\sqrt{\frac{\rho}{s(\rho+s)}} = \sqrt{\frac{a}{s(a\sin\theta+s\cos\theta)}},$$

as noted previously in Eq. (38e). The diffraction coefficient D_{p}^{s}, and the attenuation constant α_{p}^{s} are indicated in Reference [8] for the spherical surface. The geometrical details pertaining to the GTD ray description of Eq. (39) for $u_{s}(P)$ are the same as those in Fig. 7c. If

$$\frac{\rho}{s(\rho+s)} < 0,$$

then $$\sqrt{\frac{d\eta_o}{d\eta}}\sqrt{\frac{\rho}{s(\rho+s)}}$$

must be interpreted as

$$\left|\sqrt{\frac{d\eta_o}{d\eta}}\sqrt{\frac{\rho}{s(\rho+s)}}\right| e^{i\pi/2}$$

due to the crossing of a caustic.

It is evident from the results in Eqs. (38a), (38b), and (39) that a caustic of the diffracted rays is present for $\phi=\pi$ (and $\alpha=-\sin^{-1}\frac{a}{d}$ in Eq. (38a)). One notes that on crossing the caustic which occurs at $\phi=\pi$ (i.e., along the negative x-axis),two additional diffracted rays which creep around either side of the cylindrical surface also contribute to the field at P; the field of these rays is easily calculated by GTD. The caustic field may be assumed to result from the radiation by equivalent half-ring electric and magnetic currents in which the half-ring is formed by the locus of the points of diffraction of the rays shed from the hemispherical cap to the field point P for which $\phi=\pi$. The equivalent ring current concept[8,14,15,16] proves to be a useful tool for evaluating the proper field behavior at and in the vicinity of a caustic.* Such an alternative field representation for the caustic region is necessary because the simple field description of Eqs. (38ab) and (39) fails in this region (the results of Eqs. (38a) and (39) become infinite at the caustic). The transition from the single diffracted ray arriving at P in the shadow region (whose field is given by Eq. (39)) before crossing the caustic to the three diffracted rays which arrive at P in the shadow region after crossing the caustic (the three rays result from the ray corresponding to Eq. (39) shed from the hemispherical cap to P plus the two additional rays which creep around either side of the cylindrical surface before being shed towards P) will not be treated in the present report. This transition is described by the solution obtained from the equivalent current concept for the caustic region. The caustic field analysis will be completed in a future report.

Numerical Results - The near field patterns for the hemispherically capped cylinder of Fig. 12 for a radius of ka=10 and observation distance of $k\rho=100$ are presented in Figs. 13a and 13b, when this structure is illuminated by a TE_z or TM_z type plane wave, respectively. The various fields are represented as done previously for the 2-D problem. As can be seen the transition solution blends well with the geometrical optics field for both the hard and soft cases. The presence of the caustic at $\phi=\pi$,

*A study of the caustic due to the curved screen Kirchhoff diffraction term (i.e., for $\alpha=\sin^{-1}$ a/d in Eq. (38a) when $\phi=\pi$) will also be completed in a future report.

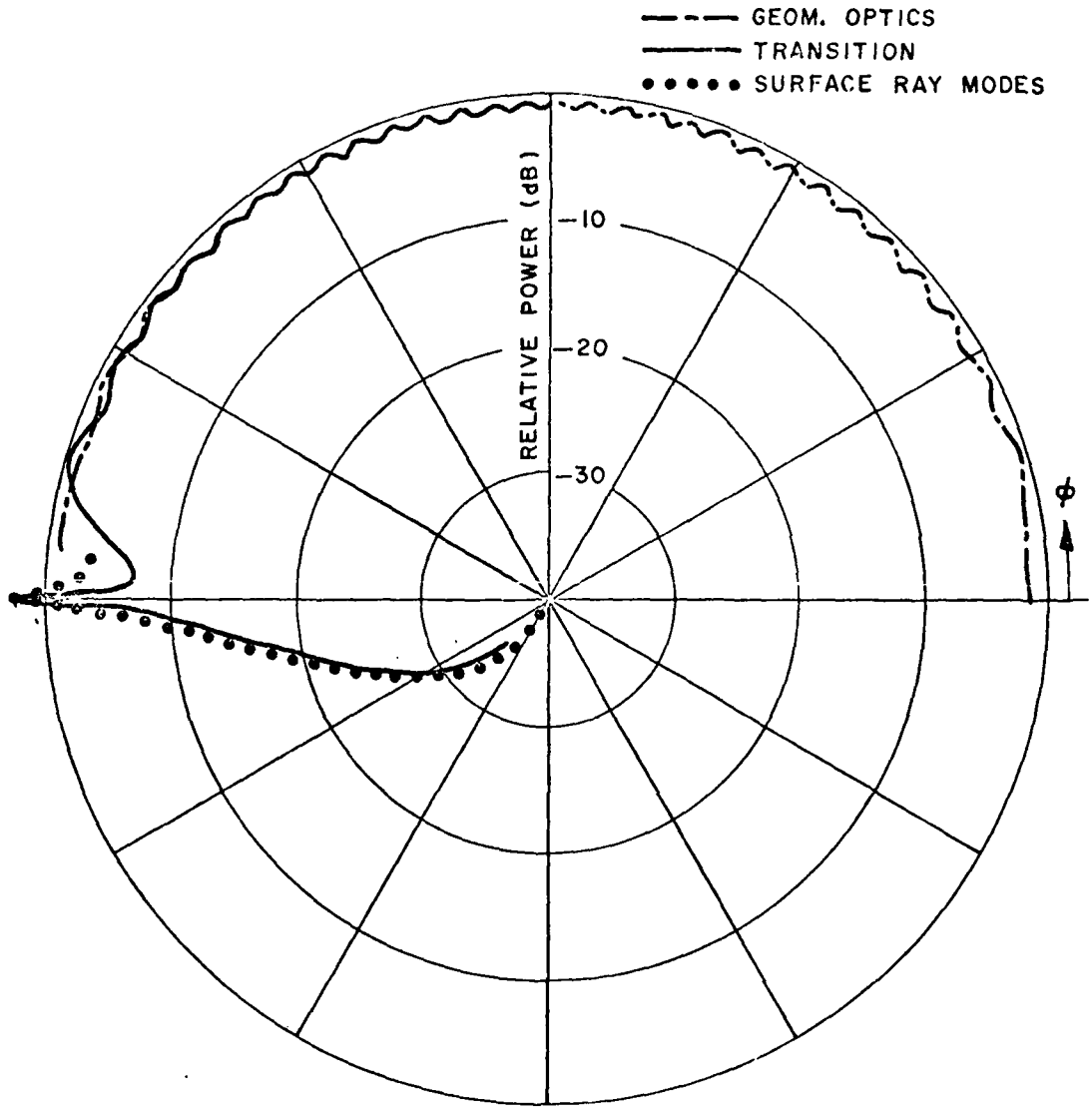

Fig. 13a. Near field pattern of hemispherically capped cylinder, hard case, ka=10, kρ=100.

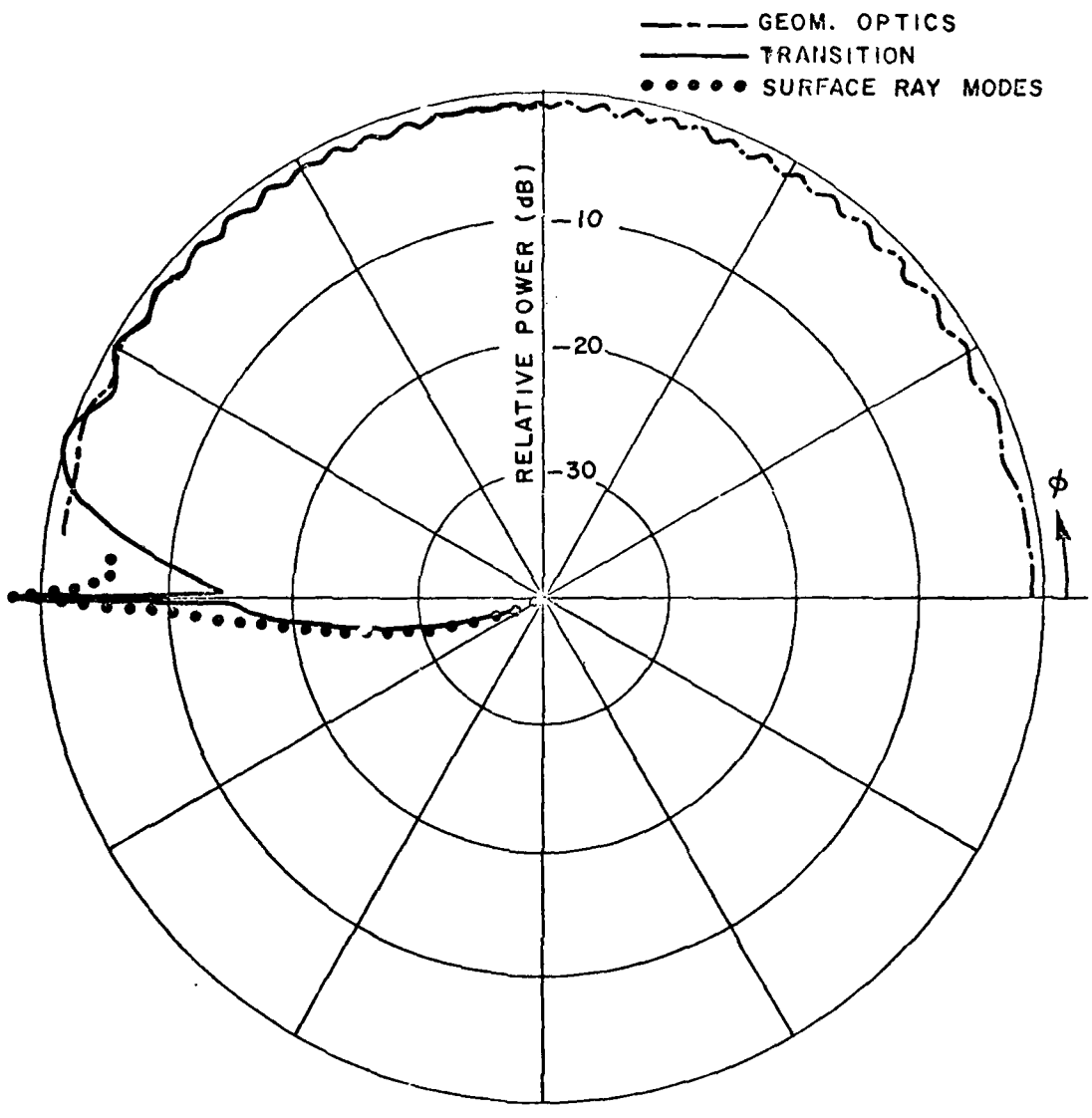

Fig. 13b. Near field pattern of hemispherically capped cylinder, soft case, ka=10, kρ=100.

however, interferes with the blending of the transition solution with the field of the surface ray modes. As stated above, the singularity due to the caustic can be easily corrected; however, this has not been done here but will be completed in a future report. When this caustic correction is incorporated, it is expected that the blending of the transition solution with the surface ray GTD solution will be as good as that indicated earlier for the 2-D problem.

IV. CONCLUSIONS

The object of this report has been to develop the complete solutions for the fields scattered by curved surfaces illuminated by near zone antennas. Specifically the high frequency solutions for curved surfaces have been completed for several years except for a transition solution which is needed around the shadow boundaries. An approximate transition region asymptotic solution is presented and developed in such a form that it can be extended to arbitrary curved surfaces. Combining this solution with the geometrical optics term in the lit region, and the geometrical theory of diffraction term in the shadow region, should provide a complete high frequency solution for the scattered fields of antennas illuminating curved surfaces in the near zone.

The solution is presented in terms of the thick half plane with a cylindrical cap showing how the various terms blend together in each region. The transition region solution developed here (Eqs. (33) and (38a)) can be shown to analytically reduce to the GTD surface ray mode solution as $F(X)\to 1$ in the shadow region sufficiently far from the shadow boundary. We have not yet shown that this transition solution can analytically reduce to the geometrical optics reflected field as $F(X)\to 1$ in the illuminated region sufficiently far from the shadow boundary. However, the numerical results presented indicate that the transition region solution does indeed blend very nicely with the GTD and the

geometrical optics solutions. Although the present transition region solution appears to be fairly accurate, it would be desirable to obtain a transition region solution from a more rigorous asymptotic analysis of the canonical circular cylinder scattering problem.

Even though the solution presented describes the one term as being a Kirchhoff solution, one can, also, show that this term can result using the GTD edge diffraction coefficient instead of the Kirchhoff edge diffraction coefficient. Using this approach the values of the transition solution do not change much near the shadow region, but they might provide improvements away from the shadow boundary. This approach will be investigated for the spherically capped cylinder in the caustic region in that in this sector the Kirchhoff and GTD solutions are observably different.

While the transition solution is being completed, the solution for a finite elliptic cylinder will be developed. This solution will provide a versatile model for the fuselage when the antenna is not mounted directly on it, i.e., such as wing or pod mounted antennas. It can, also, be used to examine the scattering effects of stores, etc. With the completion of this solution, one should have all the necessary theoretical tools to analyze any high frequency on-aircraft antenna pattern using a reasonable model representation of the actual aircraft.

APPENDIX I

EVALUATION OF THE INTEGRALS FOR THE FIELD IN THE TRANSITION REGION

A summary of the details concerning the asymptotic evaluation of the integrals in Eqs. (7a) and (7b) of Section II is provided in this appendix. The TM_z case (corresponding to Eq. (7a)) is considered first; it is followed by the TE_z case (of Eq. (7b)).

TM_z case: Employing Eqs. (9a) and (13) in Eq. (7a) leads to:

$$(A\text{-}1) \qquad u_s^s(P) \approx -\int_0^{2\pi}\left[-\frac{i}{4}\sqrt{\frac{2}{\pi k\rho}}\, e^{-i(k\rho-\frac{\pi}{4})} e^{ika\cos(\phi-\phi')}\right] \sum_{\ell=0}^{\infty} - k\left(\frac{2}{ka}\right)^{1/3}\left[\tilde{g}(\hat{\xi}_1)e^{-ika\hat{\psi}_1} + \tilde{g}(\hat{\xi}_2)e^{-ika\hat{\psi}_2}\right] a\,d\phi'.$$

Let

$$(A\text{-}2) \qquad I_1 \equiv \sum_{\ell=0}^{\infty} \int_0^{2\pi} \tilde{g}(\hat{\xi}_1) e^{-ika\hat{\psi}_1 + ika\cos(\phi-\phi')}\, d\phi';$$

$$(A\text{-}3) \qquad I_2 \equiv \sum_{\ell=0}^{\infty} \int_0^{2\pi} \tilde{g}(\hat{\xi}_2) e^{-ika\hat{\psi}_2 + ika\cos(\phi-\phi')}\, d\phi',$$

then Eq. (A-1) may be written as:

$$(A\text{-}4) \qquad u_s^s(P) \approx -\frac{i}{2}\sqrt{\frac{2}{\pi k\rho}}\, e^{-i(k\rho-\frac{\pi}{4})} \cdot \left(\frac{2}{ka}\right)^{-2/3} [I_1 + I_2]$$

with the understanding that only the $\ell=0$ term is of interest for the reason mentioned in Section II. The integral I_1, of Eq. (A-2) is evaluated first. One begins by incorporating Eq. (10a) in Eq. (A-2); thus:

$$(A\text{-}5) \qquad I_1 = \frac{1}{\sqrt{\pi}} \sum_{\ell=0}^{\infty} \int_0^{2\pi} d\phi' \int_{\Gamma_1} d\tau \, \frac{e^{-i\hat{\xi}_1\tau}}{w_2(\tau)} \, e^{-ika(\phi' - \frac{\pi}{2}) + ika\cos(\phi-\phi')}$$

with $\hat{\xi}_1 = (\frac{ka}{2})^{1/3} \hat{\psi}_1$. The sum on ℓ can be incorporated in the ϕ' integration if one changes the limits of integration to $-\infty<\phi'<\infty$, since the stationary points occur at $\phi'=\phi-(4\ell-1)\pi/2\equiv\phi_s'$. Expanding the exponential $e^{-ika[(\phi'-\pi/2)-\cos(\phi-\phi')]}$ in Eq. (A-5), about the stationary point ϕ_s' corresponding to $\ell=0$ only (since multiple encirclements are neglected), and retaining terms only to the third power in $(\phi'-\phi_s')$, one obtains:

$$I_1 \approx \frac{1}{\sqrt{\pi}} \int_{-\infty}^{\infty} d\phi' \int_{\Gamma_1} d\tau \left[\frac{e^{-i(\frac{ka}{2})^{1/3}(\phi'-\pi/2)\tau}}{w_2(\tau)} \right] e^{-ika(\phi-\pi)} e^{\frac{-ika}{6}(\phi'-\phi_s')^3},$$

or

$$(A\text{-}6) \qquad I_1 \approx \frac{e^{-ika(\phi-\pi)}}{\sqrt{\pi}} \int_{\Gamma_1} d\tau \, \frac{e^{-i(\frac{ka}{2})^{1/3}(\phi-\pi)\tau}}{w_2(\tau)} \cdot$$

$$\cdot \int_{-\infty}^{\infty} d\phi' \, e^{-i(\frac{ka}{2})^{1/3}(\phi'-\phi_s')\tau - i(\frac{ka}{6})(\phi'-\phi_s')^3},$$

after re-arranging terms, and interchanging the orders of integration. Introducing a change of variables:

$$(A\text{-}7) \qquad (\frac{ka}{2})^{1/3}(\phi'-\phi_s') = \gamma \, ,$$

allows one to simplify Eq. (A-6) to:

$$(A\text{-}8) \qquad I_1 \approx \frac{e^{-ika(\phi-\pi)}}{\sqrt{\pi}} \int_{\Gamma_1} d\tau \, \frac{e^{-i(\frac{ka}{2})^{1/3}(\phi-\pi)\tau}}{w_2(\tau)} \, (\frac{ka}{2})^{-1/3} \int_{-\infty}^{\infty} d\gamma \, e^{-i(\tau\gamma + \frac{\gamma^3}{3})}$$

One notes that the integral on γ yields the Miller type Airy function[13] denoted by $Ai(\tau)$; specifically:

$$(A\text{-}9) \qquad \frac{1}{\sqrt{\pi}} \int_{-\infty}^{\infty} d\gamma \; e^{-i(\tau\gamma + \frac{\gamma^3}{3})} \equiv 2\sqrt{\pi}\, Ai(\tau) \equiv 2\, V(\tau).$$

Defining the function $p^*(\xi)$ introduced in Section II, namely[4]:

$$(A\text{-}10) \qquad p^*(\xi) \equiv \frac{1}{\sqrt{\pi}} \int_{\Gamma_1} e^{-i\xi\tau} \frac{V(\tau)}{w_2(\tau)}\, d\tau + \frac{1}{2\sqrt{\pi}\xi} \quad ,$$

one may now rewrite Eq. (A-8) in terms of Eq. (A-9), and Eq. (A-10) as:

$$(A\text{-}11) \qquad I_1 \sim 2e^{-ika(\phi-\pi)}\sqrt{\pi}\, (\frac{ka}{2})^{-1/3} \left[p^*(\xi_1) - \frac{1}{2\sqrt{\pi}\xi_1} \right] \quad ,$$

where

$$(A\text{-}12) \qquad \xi_1 \equiv (\frac{ka}{2})^{1/3}(\phi-\pi) \quad .$$

A similar analysis for I_2 in Eq. (A-3) leads to:

$$(A\text{-}13) \qquad I_2 \sim 2e^{ika(\phi-\pi)}\sqrt{\pi}\, (\frac{ka}{2})^{-1/3} \left[p^*(\xi_2) - \frac{1}{2\sqrt{\pi}\xi_2} \right]$$

where

$$(A\text{-}14) \qquad \xi_2 \equiv -(\frac{ka}{2})^{1/3}(\phi-\pi).$$

Incorporating Eqs. (A-11) and (A-13) in Eq. (A-4) leads finally to:

$$(A\text{-}15) \qquad u_s^s(P) \sim -\frac{e^{-ik\rho}}{\sqrt{\rho}} \left[\left\{ \sqrt{\frac{2}{\pi k}}\, e^{i\pi/4}\, \frac{\sin ka(\phi-\pi)}{(\phi-\pi)} \right\} + \right.$$

$$\left. + e^{-i\pi/4} \sqrt{\frac{2}{k}}\, (\frac{ka}{2})^{1/3} \left\{ p^*(\xi_1) e^{-ika\psi_1} + p^*(\xi_2) e^{-ika\psi_2} \right\} \right]$$

where ψ_1 and ψ_2 are defined in Eqs. (17a) and (17b). The result in Eq. (A-15) corresponds to that indicated in Eq. (15).

TE_z case: Employing Eq. (9b) and Eq. (14) in Eq. (7b) leads to:

$$(A\text{-}16) \qquad u_h^s(P) \approx a \int_0^{2\pi} d\phi' \, \frac{k}{4}\sqrt{\frac{2}{\pi k\rho}} \cos(\phi-\phi') \, e^{-i\left(k\rho-\frac{\pi}{4}\right)} \, e^{ika\cos(\phi-\phi')} \cdot \sum_{\ell=0}^{\infty} \left[g(\hat{\xi}_1) \, e^{-ika\hat{\psi}_1} + g(\hat{\xi}_2) \, e^{-ika\hat{\psi}_2} \right] .$$

Let:

$$(A\text{-}17) \qquad \hat{I}_1 \equiv \sum_{\ell=0}^{\infty} \int_0^{2\pi} g(\hat{\xi}_1) \, e^{-ika\hat{\psi}_1+ika\cos(\phi-\phi')} \cos(\phi-\phi')d\phi';$$

$$(A\text{-}18) \qquad \hat{I}_2 \equiv \sum_{\ell=0}^{\infty} \int_0^{2\pi} g(\hat{\xi}_2) \, e^{-ika\hat{\psi}_2+ika\cos(\phi-\phi')} \cos(\phi-\phi')d\phi',$$

then Eq. (A-16) may be written as:

$$(A\text{-}19) \qquad u_h^s(P) \approx \left(\frac{ka}{2}\right) \frac{1}{2}\sqrt{\frac{2}{\pi k\rho}} \, e^{-i\left(k\rho-\frac{\pi}{4}\right)} \, [\hat{I}_1 + \hat{I}_2].$$

Following the procedure for the TM_z case, one may write $\hat{I}_1$ in terms of the stationary point at $\phi_s'=\phi-\pi/2$ (corresponding to the $\ell=0$ term) as:

$$(A\text{-}20) \qquad \hat{I}_1 \approx \int_{-\infty}^{\infty} g(\hat{\xi}_1)(\phi'-\phi_s') e^{-ika(\phi-\pi)-i\frac{ka}{6}(\phi'-\phi_s')^3} d\phi' \quad ,$$

where $\cos(\phi-\phi')$ in Eq. (A-17) has been approximated by $(\phi'-\phi_s')$ in the neighborhood of the stationary point, and the limits of integration have been changed to $|\phi'|<\infty$ as done for the TM_z case. Incorporating Eq. (10b) into Eq. (A-20) gives:

$$(A\text{-}21)\quad \hat{\Upsilon}_1 \approx \frac{1}{\sqrt{\pi}} \int_{-\infty}^{\infty} d\phi' \int_{\Gamma_1} d\tau \, \frac{e^{-i\left(\frac{ka}{2}\right)^{1/3}\tau(\phi' - \frac{\pi}{2})}}{w_2'(\tau)} \, (\phi' - \phi_s') e^{-ika(\phi-\pi) - i\frac{ka}{6}(\phi'-\phi_s')^3}$$

$$= \frac{e^{-ika(\phi-\pi)}}{\sqrt{\pi}} \int_{\Gamma_1} d\tau \, \frac{e^{-i\left(\frac{ka}{2}\right)^{1/3}\tau(\phi-\pi)}}{w_2'(\tau)} \cdot$$

$$\cdot \int_{-\infty}^{\infty} d\phi' \, e^{-i\left(\frac{ka}{2}\right)^{1/3}(\phi'-\phi_s')\tau - i\left(\frac{ka}{6}\right)(\phi'-\phi_s')^3} (\phi' - \phi_s').$$

Introducing Eq. (A-7) into Eq. (A-21) yields:

$$(A\text{-}22)\quad \hat{\Upsilon}_1 \approx \frac{e^{-ika(\phi-\pi)}}{\sqrt{\pi}} \int_{\Gamma_1} d\tau \, \frac{e^{-i\left(\frac{ka}{2}\right)^{1/3}\tau(\phi-\pi)}}{w_2'(\tau)} \left(\frac{ka}{2}\right)^{-2/3} \int_{-\infty}^{\infty} d\gamma \gamma e^{-i\left(\tau\gamma + \frac{\gamma^3}{3}\right)} .$$

One recognizes the integral on γ to be related to the derivative of the *Airy function* $Ai(\tau)$; *namely*[13]:

$$(A\text{-}23)\quad \frac{1}{\sqrt{\pi}} \int_{-\infty}^{\infty} d\gamma \gamma e^{-i\left(\tau\gamma + \frac{\gamma^3}{3}\right)} \equiv 2i\sqrt{\pi}\, Ai'(\tau) \equiv 2i\, V'(\tau).$$

One also defines the function $q^*(\xi)$ introduced in Section II; namely[4]:

$$(A\text{-}24)\quad q^*(\xi) \equiv \frac{1}{\sqrt{\pi}} \int_{\Gamma_1} e^{-i\xi\tau} \frac{V'(\tau)}{w_2'(\tau)} \, d\tau + \frac{1}{2\sqrt{\pi}\xi} .$$

Incorporating Eqs. (A-23) and (A-24) in Eq. (A-22) finally gives:

$$(A\text{-}25)\quad \hat{\Upsilon}_1 \approx e^{-ika(\phi-\pi)} \sqrt{\pi} 2i \left(\frac{ka}{2}\right)^{-2/3} \left[q^*(\xi_1) - \frac{1}{2\sqrt{\pi}\xi_1} \right] ,$$

with ξ_1 defined in Eq. (A-12). A similar analysis for $\hat{\Upsilon}_2$ leads to:

$$(A\text{-}26)\quad \hat{\Upsilon}_2 \approx e^{ika(\phi-\pi)} \sqrt{\pi} 2i \left(\frac{ka}{2}\right)^{-2/3} \left[q^*(\xi_2) - \frac{1}{2\sqrt{\pi}\xi_2} \right] .$$

with ξ_2 defined in Eq. (A-14). Employing Eqs. (A-25) and (A-26) in Eq. (A-19) gives

$$(A\text{-}27) \qquad u_h^s(P) \sim -\frac{e^{-ik\rho}}{\sqrt{\rho}} \left[\left\{ \sqrt{\frac{2}{\pi k}}\, e^{i\pi/4}\, \frac{\sin ka(\phi-\pi)}{(\phi-\pi)} \right\} + \right.$$

$$\left. + e^{-i\pi/4} \sqrt{\frac{2}{k}} \left(\frac{ka}{2}\right)^{1/3} \left\{ q^*(\xi_1)\, e^{-ika\psi_1} + q^*(\xi_2)\, e^{-ika\psi_2} \right\} \right]$$

with ψ_1 defined in Eq. (17a) and Eq. (17b). The result in Eq. (A-27) corresponds to the desired result indicated in Eq. (16).

APPENDIX II
KIRCHHOFF DIFFRACTION BY A HALF-PLANE

A plane wave field u^i is incident on the half-plane at y=0 for x>0 as indicated in Fig. A-1. In this appendix, the expression for the

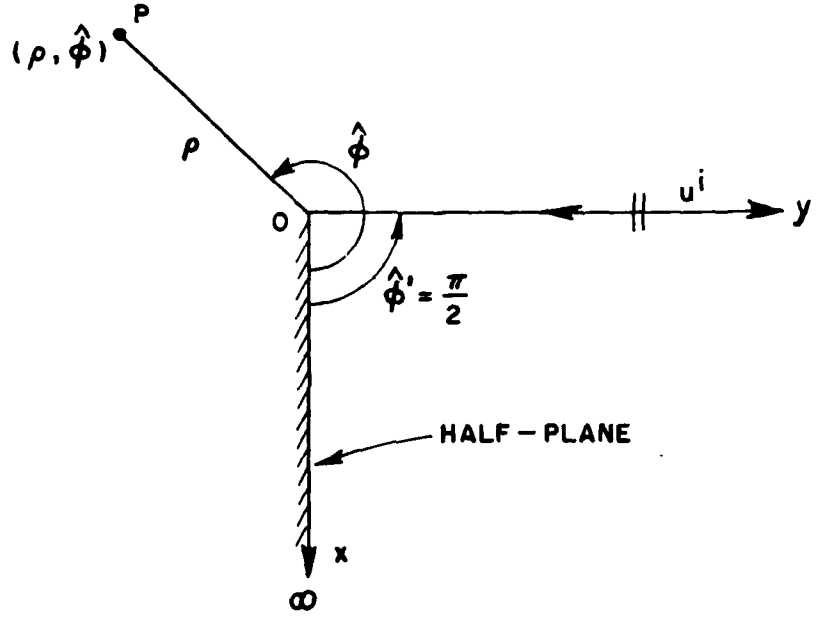

Fig. A-1. Half-plane geometry.

field diffracted by the edge (at 0) of the half-plane is derived by using a Kirchhoff approximation. Only the significant details of the analysis are indicated. It may be verified that an application of the 2-D Green's theorem to the region surrounding the half-plane leads to the following integral equation for the electric surface current density, J_s induced on the half plane when a plane wave consisting of a z-directed electric field (TM_z case) is incident on it[17]:

$$u(P) = -i\omega\mu \int_0^\infty G_0(x,y|x',0)\, J_s\,(x',0)\, dx' \qquad \text{(A-28)}$$

where G_0 is the 2-D free space Green's function, and

$$i\omega\mu J_s(x',0) = \frac{\partial u}{\partial y'}(x',0^+) - \frac{\partial u}{\partial y'}(x',0^-) \quad ,$$

(Note: surface current density J_s is z-directed.) $u(x,y)$ represents the scattered z-directed electric field surrounding the half-plane. The geometrical optics approximation allows one to let

$$\frac{-1}{i\omega\mu}\frac{\partial u}{\partial y'}(x',0^+) \approx 2\frac{\sin\hat{\phi}'}{Z_0} e^{ikx'\cos\hat{\phi}'} \quad ,$$

and

$$\frac{-1}{i\omega\mu}\frac{\partial u}{\partial y'}(x',0^-) \approx 0.$$

Employing this approximation in Eq. (A-28) gives:

$$\text{(A-29)} \qquad u(P) \approx -i\omega\mu \int_0^\infty G_0(x,y|x',0)\frac{2\sin\hat{\phi}}{Z_0} e^{ikx'\cos\hat{\phi}'}\, dx'$$

$$= -2ik\sin\hat{\phi}' \int_0^\infty G_0(x,y|x',0)\, e^{ikx'\cos\hat{\phi}'}\, dx'.$$

(Note: $k = \omega\sqrt{\mu\varepsilon}$ = free space wave number, and Z_0 = free space wave impedance = $\sqrt{\mu/\varepsilon}$.) The representation for G_0 chosen here is different from that used in Reference [17] for solving the same problem (however, the various alternative representations for G_0 may be obtained via the use of the techniques for construction of Green's functions which are also given in Reference [17]); hence, the method for solving Eq. (A-29) differs from that in Reference [17]. In the present analysis, the following expression is employed for G_0:

$$\text{(A-30)} \qquad G_0 = \frac{1}{4\pi i}\int_{-\infty}^{\infty} \frac{e^{-ik_x|x-x'|-i\sqrt{k^2-k_x^2}|y-y'|}}{\sqrt{k^2-k_x^2}}\, dk_x \quad , \qquad -\pi<\arg k_x<0.$$

Incorporating Eq. (A-30) in Eq. (A-29) gives:

$$(A\text{-}31) \qquad u(P) \approx \frac{-k\sin\hat{\phi}'}{2\pi} \int_{-\infty}^{\infty} dk_x \frac{e^{-i\sqrt{k^2-k_x^2}|y|-ik_x x}}{\sqrt{k^2-k_x^2}} \int_0^{\infty} dx' \, e^{ik_x x'+ikx'\cos\hat{\phi}'} .$$

The integral

$$\int_0^{\infty} dx' \, e^{ik_x x'+ikx'\cos\hat{\phi}'}$$

in Eq. (A-31) gives the result

$$\frac{i}{k_x+k\cos\hat{\phi}'}$$

(Here $k = k_1 - ik_2$ where the loss $k_2 << k_1$ and $k_1 > 0$. The loss is added for ease of analysis; k_2 may be set equal to zero in the final solution.) Thus, Eq. (A-31) becomes:

$$(A\text{-}32) \qquad u(P) \approx \frac{-ik\sin\hat{\phi}'}{2\pi} \int_{-\infty}^{\infty} dk_x \frac{e^{-i\sqrt{k^2-k_x^2}|y|-ik_x x}}{\sqrt{k^2-k_x^2}\cdot(k_x+k\cos\hat{\phi}')} .$$

The integral in Eq. (A-32) may be evaluated by the steepest descent method which includes the Pauli-Clemmow modification[10] (for a pole near a saddle point) after employing the polar transformations $k_x = k\cos\alpha$, and $k_y = +k\sin\alpha$. The integral in Eq. (A-32) is thus transformed into a contour integral in the complex α-plane as:

$$(A\text{-}33) \qquad u(P) \approx \frac{i\sin\hat{\phi}'}{2\pi} \int_C \frac{e^{-ik\rho\cos(\alpha\mp\hat{\phi})}}{\cos\alpha+\cos\hat{\phi}'} \, d\alpha \quad , \quad \begin{matrix} 0<\hat{\phi}<\pi \\ \pi<\hat{\phi}<2\pi \end{matrix} .$$

The contour of integration C for Eq. (A-33) is shown in Fig. A-2. Since $\hat{\phi}' = \pi/2$ in the present problem, Eq. (A-33) becomes for $0<\hat{\phi}<\pi$ (the results for $\pi<\hat{\phi}<2\pi$ are symmetric about $\hat{\phi}=\pi$):

$$u(P) \approx \frac{i}{2\pi} \int_C \frac{e^{-ik\rho\cos(\alpha-\hat{\phi})}}{\cos\alpha}\, d\alpha \,. \tag{A-34}$$

The integration contour C may be deformed onto the steepest descent path (SDP) through the saddle point at $\alpha=\hat{\phi}\equiv\alpha_s$ as indicated in Fig. A-2.

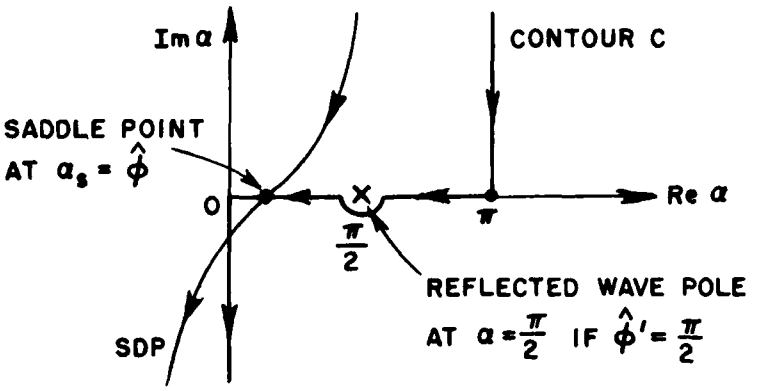

Fig. A-2. Contour of integration in the complex α-plane.

The reflected wave pole is crossed if $\alpha_s<\pi/2$ and its contribution (residue) must be included. The saddle point contribution to SDP gives the desired diffracted field; without giving details of the SDP evaluation (which are available for the wedge diffraction problem in Reference [10]), the result for the diffracted field u^d is:

$$u^d \sim \frac{\mp 2}{\cos\hat{\phi}} \left\{ \frac{-i}{4}\sqrt{\frac{2}{\pi k\rho}}\, e^{-i\left(k\rho-\frac{\pi}{4}\right)} \right\} \cdot F(X) \,, \quad \begin{matrix} \hat{\phi}<\pi \\ \hat{\phi}>\pi \end{matrix} \tag{A-35}$$

where F(X) is defined in Eq. (23) of Section II; here X is given by:

$$X = 2k\rho\cos^2\left[\frac{(\hat{\phi}-\frac{\pi}{2})}{2}\right] . \tag{A-36}$$

Converting the result of Eq. (A-35) (which is valid for the coordinate system of Fig. A-1) to a result that is valid in the coordinate system of Fig. A-3 in which $\phi=\hat{\phi}-\frac{\pi}{2}$ and $\phi'=\hat{\phi}'-\frac{\pi}{2}=0$ (for $\hat{\phi}'=\frac{\pi}{2}$), one obtains:

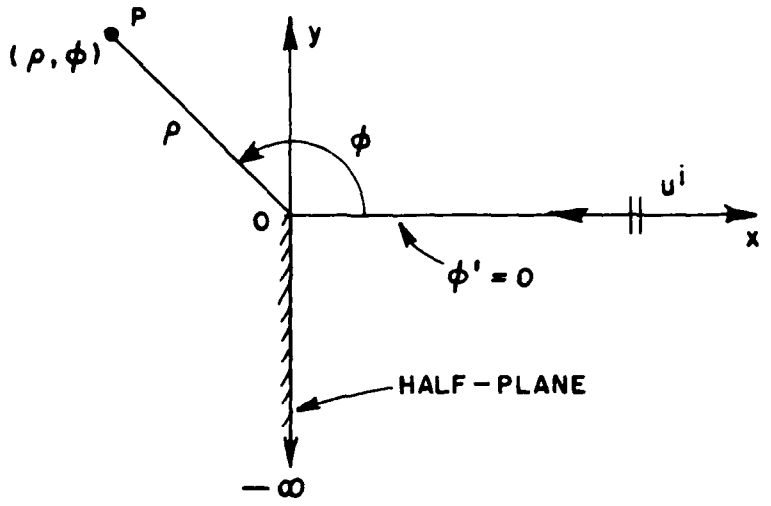

Fig. A-3. Transformed coordinate system for the half-plane problem.

$$(A\text{-}37)\qquad u^d(P) \sim -\frac{2}{\sin\phi}\left\{-\frac{i}{4}\sqrt{\frac{2}{\pi k}}\,e^{i\pi/4}\right\} F(2k\rho\cos^2\tfrac{\phi}{2})\,\frac{e^{-ik\rho}}{\sqrt{\rho}}$$

$$\equiv D_k(\phi)\,\frac{e^{-ik\rho}}{\sqrt{\rho}}$$

in which, the Kirchhoff diffraction coefficient, $D_k(\phi)$ is

$$(A38a)\qquad D_k(\phi) \equiv \left(-\frac{i}{4}\sqrt{\frac{2}{\pi k}}\,e^{i\pi/4}\right)\left(\frac{-2}{\sin\phi}\right)\,F(X)$$

where

$$(A\text{-}38b)\qquad X = 2k\rho\cos^2\frac{\phi}{2}\ .$$

The result in Eq. (A-38a) checks with that given in Eq. (22) of Section II. The $u^d(P)$ for the TE_z case is assumed to be the same as in (A-37); this assumption is reasonable within the transition region near $\phi=\pi$, where the Kirchhoff result is relatively insensitive to polarization effects.

REFERENCES

1. Burnside, W.D., "Analysis of On-Aircraft Antenna Patterns," Report 3390-1, August 1972, ElectroScience Laboratory, Department of Electrical Engineering, The Ohio State University; prepared under Contract N62269-72-C-0354 for Naval Air Development Center.

2. Marhefka, R.J., "Roll Plane Analysis of On-Aircraft Antennas," Report 3188-1, December 1971, ElectroScience Laboratory, Department of Electrical Engineering, The Ohio State University; prepared under Contract N62269-71-C-0296 for Naval Air Development Center.

3. Burnside, W.D., "Analysis of On-Aircraft Antenna Patterns," Report 3390-2, May 1973, ElectroScience Laboratory, Department of Electrical Engineering, The Ohio State University; prepared under Contract N62269-72-C-0354 for Naval Air Development Center.

4. Logan, Nelson A., "General Research in Diffraction Theory," Vol. 1, Report LMSD-288087, Missiles and Space Division, Lockheed Aircraft Corp., December 1959. (This reference contains an extensive bibliography dealing with previous work on the diffraction of waves by smooth convex surfaces).

5. Bowman, J.J., Senior, T.B.A. and Uslenghi, P.L.E. (Eds.), Electromagnetic and Acoustic Scattering by Simple Shapes, North Holland Publishing Co., 1969, (p. 103 and p. 112 list Goriainov's results).

6. Wait, J.R. and Conda, A.M., "Diffraction of Electromagnetic Waves by Smooth Obstacles for Grazing Angles," Jour. of Res., N.B.S., Vol. 63D, No. 2, Sept.-Oct., 1959, pp. 181-197.

7. Logan, Nelson A., "General Research in Diffraction Theory," Vol. 2, Report LMSD-288088, Missiles and Space Division, Lockheed Aircraft Corp., December 1959. (This reference contains tabulated values of the $p(\xi)$ and $q(\xi)$ functions).

8. Pathak, P.H. and Kouyoumjian, R.G., "The Radiation from Apertures in Curved Surfaces," Report 3001-2, December 1972, ElectroScience Laboratory, Department of Electrical Engineering, The Ohio State University; prepared under Grant NGR 36-008-144 For NASA Langley Research Center, Hampton, Virginia. (pp. 22-23 contain a description of the pseudo-ray system introduced by Kouyoumjian for the Fock current in the lit part of the penumbra region on a smooth convex surface excited by a plane wave.)

9. Keller, J.B., "Geometrical Theory of Diffraction," J. Opt. Soc. Am., Vol. 52, No. 2, February 1962, pp. 116-130.

10. Hutchins, D.L. and Kouyoumjian, R.G., "Asymptotic Series Describing the Diffraction of a Plane Wave by a Wedge," Report 2183-3, December 1959, ElectroScience Laboratory, Department of Electrical Engineering, The Ohio State University; prepared under Contract AF19(628)-5929 for Air Force Cambridge Research Laboratories. (AD 699 228).

11. Kouyoumjian, R.G., "Asymptotic High Frequency Methods," Proc. IEEE, 53, 1965, pp. 864-876.

12. Kouyoumjian, R.G. and Pathak, P.H., "The Dyadic Diffraction Coefficient for a Curved Edge," Report 3001-3, August 1973, ElectroScience Laboratory, Department of Electrical Engineering, The Ohio State University; prepared under Grant NGR 36-008-144 for NASA Langley Research Center. (A paper on this subject is currently in preparation for publication.)

13. Abramowitz and Stegum (Eds.), Handbook of Mathematical Functions, National Bureau of Standards Publication, June 1964, p. 478.

14. Ryan, C.E. and Peters, L., Jr., "Evaluation of Edge-Diffracted Fields Including Equivalent Currents for the Caustic Regions," IEEE Trans. Ant. and Prop., Vol. AP-17, No. 3, May 1969. (See corrections to this paper in March 1970 issue of IEEE Trans. AP.)

15. Ratnasiri, P.A.J., Kouyoumjian, R.G. and Pathak, P.H., "The Wide Angle Side Lobes of Reflector Antennas," Report 2183-1, March 1970, ElectroScience Laboratory, Department of Electrical Engineering, The Ohio State University; prepared under Contract AF 19(628)-5929 for Air Force Systems Command. (AFCRL-69-0413) (AD 707 105)

16. Burnside, W.D. and Peters, L., Jr., "Axial Radar Cross Section of Finite Cones by Equivalent Current Concept with Higher Order Diffraction, Radio Science, Vol. 7, No. 10, October 1972, pp. 943-948.

17. Felsen, L.B. and Marcuvitz, Radiation and Scattering of Waves, Prentice-Hall, Inc., 1973, pp. 721-724.


DATE
ILME